Stratigraphic and structural controls on groundwater flow in an outcropping fossil fan delta: the case of Sant Llorenç del Munt range (NE Spain)

Marc Anglés[(1)], Albert Folch[(2,3)], Oriol Oms[(4)], Eudald Maestro[(4)], Josep Mas-Pla[(5)]

(1) Escuela de Ingeniería de Procesos Industriales, Facultad de Ingeniería, Universidad Católica de Temuco, 4510721 Temuco, Chile. E-mail: marc.angles@outlook.es

(2) Departament d'Enginyeria Civil i Ambiental, Universitat Politècnica de Catalunya-BarcelonaTech, 08034 Barcelona, Spain.

(3) Unitat Associada: Grup d'Hidrologia Subterrània (UPC-CSIC)

(4) Unitat d'Estratigrafia, Departament de Geologia, Facultat de Ciències, Universitat Autònoma de Barcelona, 08193 Bellaterra, Spain.

(5) Grup de Geologia Aplicada i Ambiental (GAiA), Centre de Recerca en Geologia i Cartografia Ambiental (Geocamb), Dep. de Ciències Ambientals, Universitat de Girona, and Catalan Institute for Water Research (ICRA), 17003 Girona, Spain.

Submitted to ***HydrogeologyJournal***, December 2016. Reviewed, February 2017

Abstract

Mountain regions provide hydrogeological models and opportunities to understand the role of geological factors on groundwater resources. The effects of sedimentary facies and fracture distribution on groundwater flow and resources exploitation are studied in the ancient fan delta of Sant Llorenç de Munt (Central Catalonia, Spain) by integrating geological field observations (using sequence stratigraphy methods) and hydrogeological data (pumping tests, hydrochemistry and environmental isotopes). The comprehensive analysis of data portrays the massif as a single unit, constituted by different compartments determined by specific layers and sets of fractures. Two distinct flow systems, local and a regional, are identified based on pumping test analysis as well as hydrochemical and isotopic data. Drawdown curves derived from pumping tests indicate that the behavior of the saturated layers, whose main porosity is given by the fracture network, corresponds to a confined aquifer. Pumping tests also reflect a double porosity within the system and the occurrence of impervious boundaries that support a compartmentalized model for the whole aquifer system. Hydrochemical data and its spatial evolution show the result of water-rock interaction along the flow lines. In this sense, magnesium concentration derived from dolomite dissolution, is a tracer of the flow-path along distinct stratigraphic units. Water stable isotopes indicate that evaporation (near to 5%) occurs in a wide unsaturated zone within the massif before infiltration reaches the water table. The hydrogeological analysis of this outcropping system provides evidences for the understanding of groundwater flow in similar buried systems where logging and hydrogeological information are scarce.

KEYWORDS: lithostratigraphy, geohydrology, hard-rock aquifers, hydrochemistry, stable isotopes.

1- INTRODUCTION

Groundwater is an important resource in many areas of the world because of its widespread distribution compared to that of surface water. Nevertheless, many areas rely on consolidated sedimentary rock aquifers whose hydrogeological properties are related to secondary processes such as fracturing or dissolution. Their geological architecture is hence highly heterogeneous and, therefore, it controls groundwater flow magnitude and direction along preferential flow paths.

For instance, the studies of alluvial fan aquifers are usually based on limited geological data that simply provide a general description of these systems. Such studies include the Choshui fan-delta in Taiwan (Chen and Liu 2003; 2005; Peng et al. 2014), and the Dead-Sea fan deltas (Yechieli et al. 2010). All these studies are based on subsurface data to describe rock bodies' geometry, permeability, barriers location, and other hydrogeological features. The lateral lithostratigraphic changes and the basement/boundary characteristics of these formations can largely affect groundwater flow and its quality. In this sense, lithological variations may naturally lead to the occurrence of natural substances (i.e, hardness, sulfate, sodium and/or trace elements) that affect the quality of groundwater resources (Li et al. 2014; Mas-Pla et al. 2016).

From a sedimentological point of view, alluvial fans and alluvial fan deltas have been extensively studied (Arenas et al. 2001; Benvenuti 2003; Blair 2000; DeCelles et al. 1991; Harvey et al. 2005; Sohn et al. 1999), as well as their relationship with fossil fuel

and groundwater resources (e.g., Galloway and Hobday 1996). Petroleum geology methods as facies modelling and geostatistics have also been applied to deltaic and alluvial systems such as the one studied in this paper, hence stratigraphic and sedimentological features are well known for these geological system (e.g., Cabello et al. 2011).

In order to contribute to the understanding of the hydrogeological processes in fossil fan deltas as in mountain areas, we present a stratigraphic and hydrogeological study of the Paleogene fan delta of Sant Llorenç del Munt (Barcelona, NE Spain), a well-exposed mountain range massif with extensive and clear outcrops, with numerous springs and some groundwater exploitation wells. Such particularities allow characterizing its hydrogeological system in detail as an example of these groundwater flow systems. Here, we describe a geohydrological conceptual model by integrating geology (tectonic structure, stratigraphy, lateral sedimentary changes, mapping and subsurface data) and groundwater hydrology (pumping tests, major ion hydrochemistry and environmental isotopes). We especially focus on how the overall flow pattern and water resources storage are affected by the less permeable rock types and the structural setting of the massif.

Study area

The study area is located in the SE margin of the geological Ebro Basin, and it is attached to the Catalan Costal Ranges (Fig. 1a, b). The Cenozoic Ebro basin is a foreland basin bounded by three mountain ranges: the Pyrenees to the N and the Catalan Coastal Ranges (CCR) and the Iberian Ranges to SE and SW, respectively. During the middle and late Eocene this basin was connected to the Atlantic and at the basin margin several fan deltas developed, including that of Sant Llorenç del Munt (Maestro 1987; López-Blanco 1996). Sediment source areas from SE fans were the

CCR, which constituted an Alpine fold and thrust belt containing a Varisc basement and a Mesozoic cover (Anadón et al. 1985a; 1985b; López-Blanco 1994; 2006).

The subaerial part of this delta corresponded to an alluvial fan with a proximal area dominated by gravel-size sediments, and in the distal part, sand and mud accumulated. In its submarine part, a sandy delta front and a muddy prodelta also developed. Episodes of carbonate sedimentary deposition on the shelf are also found in the stratigraphic series. Presently, all these sediments are found as cemented rocks, and they constitute an isolated mountain massif (mainly conglomerate and sandstone) of 1104 m of maximum altitude, with nearly 600 m reliefs. The massif undergoes differential erosion depending on the different resistance to denudation of its distinct sedimentary layers and tectonic elements (faults and joints).

Two distinct typologies of factures have been described in the Sant Llorenç del Munt conglomeratic formations: interjoints and megajoints (Andrés et al. 1964; Freixes 1986). Interjoints are preferentially developed in meter-thick layers that show a fragile behaviour under tectonic stress. Megajoints cross the whole conglomerate bodies with thicknesses from tens to hundreds of meters. Lithology, grain size and thickness of each lithofacies type (i.e., the sedimentary facies) define the fracture pattern, and consequently the hydraulic connectivity within each unit, as stated by Alsaker et al. (1996) for the nearby and geologically equivalent Montserrat massif conglomerates. In broad terms, fracture frequency is higher as bedding thickness and grain size decreases, creating a heterogeneous spatial (horizontal as well as vertical) distribution of porosity which is paramount to describe the hydrogeological behaviour and water resources yield of alluvial fan sedimentary formations.

Average climatic conditions in the area, accordding to the three observatories located at altitudes between 321 and 528 m asl, are mean temperature of 13.30°C, 624 mm of rainfall, and an actual evapotransporation of 488 mm, which represent a 78.3% of the

mean precipitation. Population of the municipalities included in the study area is of 58,885 inhabitants (IDESCAT 2016). Water supply relies on water transfer from other bains (Llobregat-Ter), so groundwater resources basically satisfy the 30% of the population needs. No significant agricultural demand exists in the area. Land use in the study area is mainly Mediterranean forestry (89.4%) rather than agriculture (1.2% in 2000; Grau et al. 2007)

2- METHODS

2.1- Geological methods

Acquisition of surface geology consisted in geological mapping and rock characterization. Geological mapping for the central Sant Llorenç del Munt fan delta was mainly conducted at 1:5000 scale (Anglés and Maestro 2010-2011), while for the surrounding areas we redrawed the 1:50.000 geological map (after ICGC 2003; 2010; 2011a; 2011b). The geological map is summarized in Fig. 1c and is it constitutes the basis for drawing distinct cross sections of hydrogeological interest that also include borehole information. Geological mapping and depositional system analysis have provided the identification of the main lithological units. More importantly, they have determined the spatial distribution and geometry of the main lithological units, accounting also for structural elements, such as fractures, to build up a basic geohydrological frame of the system. Field measurements of fracture densities in the sedimentary formations also complement the hydrogeological information.

Field rock description provided parameters such as lithology, conglomerate grain composition, color, texture (grain size, sorting), porosity, internal structure and morphology of rock bodies (morphology and lateral fingering of different rock types)

149 and the occurrence of fractures and joints. Representative samples from all rock types
150 were used to obtain sixteen thin sections. We applied two staining types, yellow dye to
151 visualize porosity and Alizarin red S and Potassium ferricyanide for the determination
152 of calcite (Lindholm and Finkelman 1972). Two types of porosity are observed in the
153 petrographic microscope: microfractures and, in lesser proportion, intergranular
154 porosity. Percentages of porosity vs particles and cement were evaluated with
155 comparison charts. Based on optical mineralogy the main constituents of the sandy
156 fraction and cement were identified. This provided percentages of silicate minerals,
157 calcite, dolomite and others (see details in Anglés 2013). This characterization is of
158 paramount importance to correlate rock units with hydrogeological and hydrochemical
159 features.

160

161 **2.2- Hydrogeological methods**

162 *Well testing*

163 Three pumping tests were carried out in July of 2012: S.LL-22 (300 m depth), S.LL-31
164 (335 m) and S.LL-27 (389 m). Data from two previous essays have been revisited:
165 S.LL-24 (51 m) and S.LL-25 (164 m). Tests were conducted once recovery was
166 completed from previous pumping periods. Tests consisted of pumping and recovery
167 time spans lasting between 2 and 4 hours. The hydraulic head during the test was
168 measured manually with water level meter and/or with piezometric pressure probes
169 (Mini-diver, Schlumberger).

170 *Hydrochemical sampling and analysis*

171 The hydrochemical dataset consists of 31 and 38 water samples collected during two
172 field surveys: summer 2011 and spring 2012, respectively, coinciding with periods of
173 drought and rain. Sampling points (Fig. 2) account for twenty eight natural springs and

eleven wells with depths between 4 and 389 m. Five samples of the total are not directly located on the Eocene substrate (S.LL-04, S.LL-09, S.LL.-10, S.LL-28 and S.LL.-38), but they correspond to Quaternary sedimentary deposits, most of them alluvial formations, located along the Sant Llorenç del Munt drainage network. Water stable isotopic data (oxygen-18 ($\delta^{18}O$) and deuterium (δD)) were only collected during the summer 2011 survey.

Samples for hydrochemical and isotopic analysis were taken from natural springs and active water supply wells. We ensured that at least three casing volumes were removed from each bore prior to sampling, therefore samples are an integration of all productive layers along the borehole. Physicochemical parameters (pH, electrical conductivity, and temperature) were measured in situ using a flow cell to avoid contact with the atmosphere. After filtration (0.45 μm), samples were processed in the field and stored at 4 ºC in a dark environment for subsequent transport and analyses.

In the laboratory, alkalinity (as HCO_3^-, since pH < 8.3; mean pH = 7.39±0.04 in 2011, and 7.21±0.06 in 2012) was measured by titration (METROHM 702SM Titrino). Anion (NO_3^-, SO_4^{2-} and Cl^-) content was measured by Capillary Electrophoresis (Agilent Technologies) using indirect UV detection; concentrations of Na^+, K^+, Ca^{2+} were measured by Inductively Coupled Plasma-Optical Emission Spectrometry (ICP-OES, Perkin Elmer 4300 DV). The quality of the chemical analysis was checked by performing an ionic mass balance, with an error lower than 5%. Water stable isotopes were analyzed in a Finnigan Matt Delta S Isotope Ratio Mass Spectrometer (IRMS) coupled to an automated line based on the equilibration between H-water and H_2 gas with a Pt catalyst, and between O-water and CO_2 gas following standard methods (Epstein and Mayeda, 1953). Notation is expressed in terms of δ‰ relative to the international standards V-SMOW (Vienna Standard Mean Oceanic Water) for δD and $\delta^{18}O$. The precision (≡1σ) of the samples calculated from international and internal

200 standards systematically interspersed in the analytical batches was ±1.5‰ for δD and
201 ±0.2‰ for $\delta^{18}O$.

202

203

204 **3-RESULTS**

205

206 **3.1-Geology**

207 Ten distinct rock types (i.e., lithofacies) have been identified in the Sant Llorenç del
208 Munt system (SLMS) on the basis of distinctive lithologic, mineralogical, textural and
209 hydrogeological features which are described in detail in Table 1 and summarized in
210 Figs. 3 and 4. Indeed, the main groundwater flow in the SLMS is basically dependent
211 on fractures (joints and faults, see Andrés 1964; Freixes 1986; Alsaker et al. 1996),
212 since intergranular porosity is very low (<5%).

213 The following 10 rock types, summarized in Table 1, are ordered from coarser to
214 thinner grain size (i.e, from proximal to distal sedimentary facies):

215 **1-Clast-supported polygenic conglomerate (Cp):** this is the most widespreaded
216 lithofacies of the SLMS massif (26% of its surface). The polygenic composition of its
217 grains is due to the different origin of the source rocks, mainly belonging to the
218 Variscan basement (e.g., Paleozoic phyllites and other crystalline rocks). Grains are
219 clast supported, and matrix is sandy. The cement is calcitic. Thin section
220 determinations established a microporosity value around 1-5% of the sample surface
221 (i.e., microfractures plus intergranular porosity). This lithology creates homogeneous
222 packages of massive conglomerate, facilitating the development of penetrative and
223 spaced joints and faults that easily exceed 100 meters of vertical extension.

2-Clast-supported carbonate conglomerate (Cc) account only for the 7% of the SLMS surface, but are of particular hydrogeological importance. The clast-supported carbonate conglomerate is predominantly composed (around 80% of the grains) by carbonate Mesozoic cobbles (mainly derived from Triassic rocks). Matrix is sandy and it has poor clay and silt content. The cement is calcitic. These deposits are widely spreaded throughout the alluvial fan system and each deposit has a maximum thickness of 20-30 m. They are interbedded with type Cp. Microporosity (i.e., microfractures plus intergranular porosity) is between 1 and 5% of the sample surface. Significantly, this type presents a close-spaced fracture net, that represents the sum of interjoints (Andrés 1964), which are restricted to Cc beds, plus background joints (megajoints), and other faults that affect the conglomeratic formation as a whole (Fig. 5a).

3-Grey conglomerate (Cg) has a gravel frame and a sandy matrix with few silts and clays. Its outcropping percentage in the system is around the 7% in areal extension. They are deposited in front of the distal part of all conglomerate types (Fig. 3). Laterally, they are connected to the latter and evolve to sands towards inner basin areas. They may have a dense fracture net. This is a relevant rock type for subsurface water dynamics, since it connects conglomerates with gray sandstone layers (Sg).

4-Matrix-supported polygenic conglomerate (Cmp) accounts for around the 5% of the SLMS and are found as limited layers within Cp conglomerate layers. Their fracturing pattern resembles that of the Cp. Fracture pattern is in continuity with Cp joints, except in the thicker Cmp levels.

5-Matrix-supported carbonate conglomerate (Cmc) accounts for around the 5% of the SLMS, and they are found as limited layers within Cc conglomerates. In both cases, the matrix of the Cmp and Cmc is constituted by sandy/muddy sediments of

siliceous composition. Microporosity is around 1-5%, and fractures are poorly defined (except in the small layers interbedded within Cp or Cc).

6-Breccia of Paleozoic clasts (Bp) has a small surface extension around 2% of the SLMS (Figs. 1c and 4), and, because of this, it is not actually relevant for this study. It has a muddy matrix-supported texture which is responsible for low granular porosity. Also, its internal disorganization contributes to create a poorly developed fracture net. No aquifers have been assigned in this rock type, and it is considered as an aquiclude. Detailed description of these levels is found in Anadón (1978).

7-Red sandstone and mudstone (SMr) is an interbedded type that has a very poor to moderate sorting. Accounts for around the 22% of the SLMS, and they mainly appear in the distal alluvial fan and fan fringe areas (with maximum extent of 1.5 km in front of the alluvial fan). Microporosity is around 1% (mainly microfractures). Fractures are restricted to sandy layers, and they do not propagate into the bounding mudstones.

8-Grey sandstone (Sg) has a moderate to well sorted grain size. It accounts for around the 15% of the SLMS, and these layers are arranged in thickening and coarsening upwards cycles that have a thickness of decametric order. These cycles (Fig. 3) have a succession that begins with marls (Mgb, see below) and progress towards enriched sandstone layers (strictly, Sg) to finally evolve to grey conglomerates (Cg; Fig. 5b). These cycles provide well defined Sg and Cg units vertically isolated between marl layers (Mgb, see below).

9-Grey-blue mudstone (Mgb) shows a marl composition, and it has a bulky appearance. It accounts for around the 9% of the SLMS area. Despite its loose appearance due to weathering, with a badland morphology where it outcrops, the fresh rock is cohesive and it stands as a clear groundwater flow barrier because of its low hydraulic conductivity.

10-Limestone (LM) is alternating with marls and has a packstone to grainstone texture. Matrix is micritic and, locally, is a boundstone. Stratification is massive and nodular and it provides tabular rock bodies with thickness of metric to decametric order. It accounts for around the 2% of the SLMS and laterally and basinward evolves to Sg and Mgb, respectively. Microporosity is around 1% and fractures are well developed.

As observed in Figs. 3 and 4, all these rocktypes are arranged as lateral facies changes that grade progressively from proximal alluvial conglomerates (Cp, Cc, Cmp and Cmc) to distal alluvial sandstones and mudstone (fan fringe, SMr), to delta front sandstones (Sg, Cg) and prodelta marls (Mgb). Shallow water limestones (LM) grade laterally both to Mgb and Sg. The obtained correlation based on geological data, defines the architecture of rock types Sg, Cg and Mgb (Fig. 4, cross section A-A') that is the result of the ancient sea level relative fluctuations. Sucessive regressions and transgressions forced the emplacement of the delta front as a result of relative sea level lowstands and highstands, respectively. As we will see later, the basinwards shift of Cg during maximum progradation episodes will be particularly relevant for the hydrodynamics of the system.

3.2-Hydrogeology

The lack of wells and observations points (piezometers) within the Sant Llorenç Range does not permit neither setting approximate hydraulic head values in the study area, nor defining an approximate potentiometric map for the massif. Indirect knowledge could derive form the altitude of spring occurrence (Tables S1 and S2), yet their location depends on diverse geological factors that impede reporting any reliable cartography.

Manual hydraulic head measurements or using pressure loggers have been conducted at the same supply wells where the pumping tests have been conducted. Well

300 stratigraphy, screened intervals and test details are given in Table 2, showing that
301 some wells can be understood as exploiting a multilayered aquifer of similar
302 lithological/stratigraphic characteristics in all their depths. Head values represent thus
303 an averaged value of all layers. In this sense, maximum head elevations (a.s.l.) were
304 recorded at 191 m, 325 m, and 455 m for wells S.LL-27, S.LL-22, and S.LL-31,
305 respectively, corresponding to the integrated head among all productive layers crossed
306 by the borehole. Inside the Sant Llorenç del Munt range, stratigraphic layers and
307 discontinuities produce perched aquifers that are the origin of the multiple springs
308 disseminated along the Sant Llorenç del Munt massif.

309 Continuous head records in S.LL-31 and S.LL-27 wells showed some immediate
310 response to rainfall events with a time lag of few days (1-6 days; Anglés 2013, Figs. S1
311 and S2). This suggests that pressure variations from the recharge areas are efficiently
312 registered in these wells. Despite the multilayered nature of these boreholes and their
313 daily pumping activity, some interpretations can be made. Thus, the time lag between
314 the rainfall event and the pressure increase is interpreted as the time needed for
315 recharging water to cross the unsaturated zone and treach the water table when the
316 increase of head will be recorded as a pressure increase in the well records. This is
317 consistent with the hydrochemical and isotopic data.

318 A diagnostic analysis of the pumping tests performed at constant discharge has been
319 conducted based on the logarithmic derivative of the drawdown ($\partial s/\partial \ln t$) as a function
320 of time in the log-log scale (Renard et al. 2008). The logarithmic derivative is sensitive
321 to variations of the shape of the drawdown curve, so it allows to detect behaviors that
322 will otherwise remain unnoticed. In this sense, derivative plots reveal a diminution of
323 the derivative value which is attributed to the effect of a potential double porosity of
324 geological relevance as the derivative value recovers after its former decrease (Fig. 6).
325 Double porosity responses are noticed in wells S.LL-22 and S.LL-31. In particular, well
326 S.LL-22 shows this behavior at early time (5 min), followed by progressive increase of

the derivative value. Conversely, well S.LL-31 shows a complex behavior between 15 and 50 minutes, approximately, that later recovers to a smooth curve. The double porosity effect is associated with the later smooth decrease (40-50 min), while the first unordered decrease (15-20 min) is attributed to the effect of small, local heterogeneities of the media. Pumping test at well S.LL-.27 also shows a decline in its derivative value after 30 min, attributable to a double porosity effect, yet its drawdown and derivative value abruptly increase as a result of the effect of a no-flow boundary.

Theis equation have been used to simulate drawdown at a distance similar to well radiuses, being aware that this assumption represents an approximation to the actual drawdown, reporting the fitted values of T and S using the minimum square difference criteria between observed and simulated data (Figure 6). Early time linear behavior at well S.LL-27, with an approximate slope of 0.5, is associated to a major fault intersected by the well that only influences the early behavior, as after minute 10 the aquifer shows a radial flow according to Theis model. Early time discrepancies at well S.LL-31 are due to a well-storage effect. In each case, Theis equation can thus adequately be used to estimate the hydraulic properties of the aquifer in the vicinity of the well restricted by the short duration of the tests. Nevertheless, it is geologically significant that the double porosity effect and the occurrence of a no-flow boundary (S.LL-27) have been identified throught the diagnostic analysis.

In addition, four pumping tests with variable pumping rate (Table 2, all except S.LL-.27; Fig. 7) were also calibrated using an optimization algorithm that solves Theis equation for variable linear discharge rates based on the formulation by Tsang et al. (1977) that uses Duhamel's superposition integral (Mas-Pla et al. 1999). This procedure allows a simultaneous simulation of drawdown, some of them with variable pumping rates, and recovery data at the borehole radiuses distances, as no observation wells were available nearby these production wells. According to this procedure, storage coefficient values can also be considered for the recovery analysis.

Tests at wells S.LL-22 and S.LL-31 had shorter duration (they lasted 120 and 240 min, respectively), and they were conducted, as already mentioned, under uniform withdrawal rate till the pumping ceased. Recovery was observed during the period lengths at each well. Hydraulic head simulations using fitted T and S values are able to concurrently reproduce the drawdown and the recovery limbs considering Theis assumptions, yet they fail to reproduce the maximum observed drawdown which seemed not to have attained a uniform depth by the time the pump was turned off (Fig. 7, Table 2). Based on the former analysis of drawdown derivatives, such difference between observed and simulated maximum drawdown for the best optimized T and S values at larger times is attributed to double porosity effects. In the SLMS case, it is due to a change of fracture aperture, density or connectivity (as it can be seen in Fig. 5). Fitted values using the whole drawdown ands recovery records (Fig. 7) brings out T and S values consistent with those using Theis equation on the drawdown data only (Fig. 6), indicating that, on the whole, the exploited levels behave as confined aquifers.

Pumping tests conducted at variable pumping rates in S.LL-24 and S.LL-25 wells had longer durations (24 h, each), reaching a stabilized drawdown by the end of the pumping period (Fig. 6, Table 2). In the S.LL-24 test, the deep drawdown attained at 200 min, and which seems to persist until the end of the pumping period, is not reproduced by the simulation even though well discharge variations are considered by the algorithm. This fact points out the influence of geological heterogeneity on the hydraulic response of the aquifer system, suggesting the role of discrete elements such as fractures. In the S.LL-25 well, however, the initial high drawdown caused by a pumping rate peak is well reproduced by the model, as well as the overall trend of the drawdown. This indicates that a more homogeneous rock volume is affected by this well depression cone. Its final drawdown was well reproduced in both tests, so the T and S values can be assumed to be representative of these hydrogeological units. Simulated recovery is slower than observed data in both wells.

S.LL-27 pumping test brings out a clear example of the system's heterogeneity, as already discussed in the diagnostic analysis. Drawdown shows two distinct developed curves under a steady pumping rate (Fig. 8). The increased drawdown rate observed after 70 min points out the occurrence of some impervious boundary that highly controls the flow towards the well, defining thus an aquifer of limited extent. Therefore, it would be inappropriate using Theis approach to solve for the hydrogeological parameters using the entire drawdown record. Contrarily, it is worth noting that both withdrawal segments also achieve clear straight lines in semilog plot (Fig. 8b) that permit the interpretation of the first reach using the Cooper-Jacob method. T value (T=0.70 m^2/d) is in the lower rank of those found in the other tests. The second segment indicates the existence of an impervious boundary, and it points out that this multilayer aquifer (Table 2) can be considered, at large, a true confined aquifer as drawdown data lays on a clear straight line. Furthermore, the S value is approximate and, therefore, it must be taken with caution as the S value estimated by the Cooper-Jacob method depends on the radius from the observation well to the withdrawal well, and it has been equaled to the borehole radius. Unfortunately, the pumping test did not last long enough to observe whether if a steady drawdown was finally reached. Moreover, the lack of a true observation well doesn't allow estimating the distance to the impervious boundary using the time at which the break of the slope takes place (e.g., Chapius 1994).

The highest transmissivity values are found in S.LL-22 well (T ≈ 15 m^2/d) which is drilled in conglomerates (Cp rock type; Table 2). All other wells show lower values, being the lowest found in sandstone layers (Sg) interbedded within mudstone levels (Mgb) constituting a multilayered aquifer, as in the S.LL-27 well (T ≈ 0.65 m^2/d). Consolidated strata as conglomerates and sandstones show dense fracture nets, and since their intergranular porosity is low (<0.05) but the fitted storage coefficient values are quite large (≈0.25-0.30) we thus deduce that hydraulic conductivity mainly results

408 from fractures and their interconnectivity. Nevertheless, differences between the
409 observed drawdown data and reproduced drawdown curves based on Theis
410 assumptions reveal the heterogeneity of the system, as 1) the occurrence of
411 impervious boundaries attributed to lateral facies variations, as clearly observed in the
412 S.LL-27 well; and 2) the occurrence of double porosity effects identified in the
413 diagnostic analysis of these test conducted at a constant discharge rate. Despite the
414 importance of the fracture network in the recharge dynamics, these pumping tests also
415 point out that the exploited aquifer levels mostly behave as confined aquifers,
416 underlining the role of low permeability layers (SMr and Mgb types) as confining units.

417

418 **3.3-Hydrochemistry**

419 Based on the hydrochemical datasets of the field surveys carried out in summer 2011
420 and spring 2012 (Tables S1 and S2), several groundwater hydrochemical facies are
421 defined according to their major component content and the drilled lithostratigraphic
422 unit, as summarized in Table 3. No major hydrochemical changes are observed in the
423 Pipper plot between both surveys (Fig. 9) suggesting some steadiness in the system
424 dynamics. Five hydrochemical groups are found ('A' to 'E'):

425 Hydrochemical group 'A' is mainly defined by natural spring samples with a HCO_3-Ca
426 facies that are hosted in Cp and SMr rock types. This is the dominant group, including
427 80% of the samples. Two other common characteristics of group 'A' are its relatively
428 moderate temperature (mean T: 14.7±0.2°C in 2011, and 13.7±0.4°C in 201; SM) and
429 electrical conductivity (mean EC: 702±16 µS/cm in 2011, and 694±16 µS/cm in 2012,
430 SM). Despite the considerable percentage of dolomite in Cp layers and Cc (24.2% and
431 67.3%, respectively; Table 1) groundwater samples in group 'A' have a low Mg content
432 atributed to the low solubility of dolomite with respect to calcite. The low mineralization
433 levels and the absence of dissolved Mg point out a short transit time within these

aquifer levels. Also within this group, natural springs as S.LL-06, 04, 15, and 17 show slightly higher values of Na and Cl (increments of few units of mg/L) that are attributed to weak cation exchange, as they do not actually stand out in the plots of Fig. 10. These ions cannot either be associated to agricultural practices or human sources as nitrate content is rather low (mean value 3.16±0.52 mg NO_3/L; Tables S1 and S2; Menció et al. 2016).

Hydrochemical group 'B' is represented by a single sampling point, the Marina well (S.LL-31), showing a HCO_3-Ca-Mg-Na. This well data, when compared with 'A' group, stands out by its lower Ca content, yet higher Na and Mg (Fig. 9). This fact could result from Na/Ca exchange related to clay occurrence in SMr strata, which are found interlayered within Cp units (Fig. 4; and Table 2), giving a high Na/Ca ratio (Fig. 10). However, the increase in Mg cannot be associated to the hosting lithology as its percentage of dolomite is low (1.0% in SMr; Table 1). Therefore, it must be assumed that a slow flow originated in the saturated zone of the Cp unit provides such Mg enrichment by dolomite dissolution. This hydrochemical composition, involving dolomite dissolution and cation exchange processes, derives then from a larger water-rock interaction and a longer transit time of this sample compared to those of group 'A', which is consistent on the hydraulic properties of a sandstone and mudstone formation (SMr; Fig. 11).

Group 'C' samples are generally characterized by HCO_3-Ca-Mg facies which is attributed to the mineralogy of the grey sandstone (Sg) where wells are drilled (Fig.9). Despite the general Mg enrichment shown by the group C samples, the different Mg content in samples S.LL-29 and S.LL-30, justifies gathering them into a new subgroup 'C2'. Given the low proportion of dolomite in the grey sandstones (Table 1), it is assumed that Mg content is obtained in preceding up-gradient formations, as Cp or Cc, and its subsequent flow across the delta front facies. Indeed, Sg rock types display surface efflorescences such as hexahidrite ($MgSO_4 \cdot 6H_2O$) and epsomite

461 ($MgSO_4 \cdot 7H_2O$; Mata-Perelló 1990). Such occurrence of SO_4, attributed to pyrite
462 oxidation, may enhance dedolomitization of the small dolomite content of the Sg
463 sedimentary rocks, adding some additional Mg to groundwater. Indeed, Otero et al.
464 (2007) studied the Calders and Mura streams (located 4 and 8 kilometers to the
465 northeast) which drain through similar lithologies and concluded that SO_4 originates
466 from the oxidation of pyrite which is found scattered (mineral dissemination) within the
467 marl layers. Thus, dolomite (or Mg-rich calcite) and pyrite hosted in marine rock types
468 can be dissolved by groundwater, enhanced by the occurrence of SO_4, and provide
469 such high concentrations of Mg and SO_4.

470 Likewise, group 'D' samples actually display a similar significant increase in the
471 amounts of SO_4 and Mg with respect to the former groups (Fig. 9), accompanied by an
472 increase of EC (1251±265 µS/cm in 2011, and 1135±198 µS/cm in 2012; n=3). This
473 enrichment is due to potential groundwater pathways within the aforementioned rocks
474 enhanced by dedolomitization processes within the sedimentary units of marine origin,
475 rich in SO_4 and Mg. Two distinct subgroups can be envisaged within group 'D': HCO_3-
476 Mg-Ca (subgroup 'D1'), and HCO_3-SO_4-Mg-Ca (subgroup 'D2'; Table 3). 'D1' samples
477 (i.e., S.LL-26 and S.LL-25) are located downgradient from the main recharge area (i.e.,
478 the summit of the Sant Llorenç del Munt massif) following the northwest dipping of
479 strata, and they display an increase of the overall solute content (EC = 1050 µS/cm).
480 The 'D2' subgroup is represented by the S.LL-24 well that is located in the Llobregat
481 River valley. The well profile and design, together with its geological setting (Table 2),
482 thrust aside any chance of surface water recharge due to hydraulic connectivity with
483 the Llobregat River. Thus, its higher mineralization (1768 µS/cm in 2011) with respect
484 to 'D1' (888 and 1097 µS/cm) must be result of intense subsurface water rock-
485 interaction with a distinct pathway across the different lithological layers. Large values
486 of SO_4 and Cl, and the location of these wells in the hydrogeochemical conceptual
487 scheme (Fig. 13) suggest a longer transit time.

Finally, group 'E' is only defined at the S.LL-27 deep well (389 m). It shows high EC values (1291 µS/cm in 2011, and 1217 µS/cm in 2012; n=1) and HCO_3-Na facies. Such sample also presents a high Cl content attributed to clay weathering; Ca depletion is interpreted as a result of the cationic Na/Ca exchange that takes place in clay layers (Mgb layers; Figure 10). Both, the high chloride content and intense cationic exchange, also implies long residence times (Tóth 1995; 2000; Carrillo-Rivera et al. 2007; Folch et al. 2011; Anders et al. 2013). This 'E' group also shows some SO_4 enrichment with respect to group 'A' reflecting the influence of marine rock types in groundwater hydrochemistry.

3.4-Environmental isotopes ($\delta^{18}O$, δD)

Groundwater stable isotope data (especially those of hydrochemical groups 'A' and 'B') cluster together around mean values of $\delta^{18}O$ = -8.17±0.04‰ and δD = -49.05±0.20‰, in an area located above the Global Meteoric Water Line ($\delta D = 8\,\delta^{18}O + 10$; Craig 1961; Figure 12). The closest local meteoric line was defined at the Montseny Range, about 40 km NE and at an elevation of 700 m (Neal et al. 1992). This local meteoric line ($\delta D = 7.9\pm0.4\,\delta^{18}O + 10.0\pm3.2$, n=29, r^2=0.93) assumes a d-excess enrichment as that of the mean Mediterranean Meteoric Water Line ($\delta D = 8\,\delta^{18}O + 15$) defined by Lambán and Custodio (1999). Indeed, d-excess values of these samples lays in the range between 12 and 18‰, which is also close to the range defined by Plata Bedmar (1994) for the groundwater isotopic content in Iberian Mediterranean basins, and consistent with the mentioned meteoric lines. Altitudinal isotopic gradients defined at nearby areas (Montseny range; Carmona et al. 2000; and eastern Pyrenees; Brusi et al. 2011) indicate that isotopic contents are consistent with the Sant Llorenç del Munt elevations, and that the variation of 1‰ $\delta^{18}O$ rightly covers the altitudinal difference existing between the summit and the surrounding valleys.

514 Most of the wells have their stable isotopic values arranged along a line of slope of 5
515 and an approximate origin at $\delta^{18}O$ = -8.2‰, δD = -50‰. This fact indicates that deep
516 groundwater within the massif, pertaining to longer transit times flowlines, has
517 undergone some evaporation processes that have enriched their isotopic water
518 content. Only three springs show a similar tendency. Given the geological setup of the
519 SLMS, it can be conceived that springs respond to local, perched aquifer systems at
520 distinct altitudes with a short residence time within the system. Indeed, the alluvial fan
521 formation can be understood as a stratigraphically and tectonically compartmentalized
522 system (Llopis 1944; Andrés 1964; Freixes 1986), as already deduced from the
523 pumping tests. Contrarily, wells of hundreds of meters depth are recharged by a large
524 scale regional system that, due to the local orography, presents a wide unsaturated
525 zone of hundreds of meters from the land surface to the water table. It is therefore
526 reasonable to assume that some evaporation may occur during rainfall subsurface
527 percolation along the fractures towards the water table. Deviation from the meteoric
528 line cannot be attributed to geographical effects, as continentality, since the distance
529 between the closest and further points from the Mediterranean Sea is just of 10 km.

530 According to Gonfiantini (1986) equations, the most evaporated groundwater sample
531 (that is, S.LL.30) shows an evaporation percentage around 5%, assuming an isotopic
532 composition of the atmospheric vapor of $\delta^{18}O$= -12‰, δD= -86‰, and an observed
533 mean daily relative humidity of 70.0±0.2% (Rellinars Observatory 2007-2017;
534 RURALCAT 2017). Even though the displacement from the meteoric line shown by
535 evaporated samples seems dramatic when plotted as in Fig. 12, it only stands for a
536 small percentage of water loss through evaporation in the unsaturated zone, even
537 though this 5% loss represents a large volume of water at a regional scale. Although
538 this is quantitatively inconsequential, it supports the interpretation of two distinct
539 hydrogeological systems within the SLMS from a conceptual perspective: 1) a local one
540 represented by spring data (mainly, group ‘A’), which has not undergone isotopic

fractionation, determined by the compartmentation of the main aquifers by fractures and low permeability layers, and 2) a regional system that includes the general recharge all over the mountain range. This regional system recharges the deepest aquifer layers by downward percolation through a wide vadose zone. The good alignment of well isotopic data along an evaporation trend line assumes that groundwater is largely homogenized during the infiltration process. The role of distinct fracture systems with different hydraulic behaviors as double porosity, as also observed from field outcrops, contributes to the homogenization of the infiltrating recharge reflected by the isotopic data.

Sample from geochemical group 'E' doesn't show any evaporation trend, suggesting a complex (mixed) circulation flow (see Fig. 13). Its sodium-bicarbonate facies would be caused by water-rock interaction processes occurring within the delta front environment (Sg and Mgb). This geochemical group is based on data from a single well, so complementary data could provide further information.

4- DISCUSSION AND CONCEPTUAL FLOW MODEL

Geological information compiled in the Sant Llorenç del Munt massif (Fig. 4) permits a comprehensive three-dimensional understanding of the lateral and vertical relationships among the ten rock types. Lithofacies characteristics and diversity originated as a result of sediment accumulation in each part of the alluvial fan system. Further diagenetic processes will define the degree of compaction and cementation accordding to their original textural features. Such intrinsic primary sedimentological features, altogether with fracturation pattern (Alsaker et al. 1996), determine the Sant

Llorenç de Munt hydrogeological system final structure; that is, the occurrence of distinct geohydrologic compartments at different scales. Stratigrapical and tectonic elements -namely, lithology, layer geometry and its lateral continuity, tilting and fracturing- become the key features that govern groundwater flow at the SLMS, configuring a compartmental system with two main hydrological dynamics.

Geomorphological evolution widens fracture apertures near the surface due to decompression and weathering, which will also be less intensive in depth. This implies that aquifer transmissivity will decrease in depth. Therefore, structural factors lastly define the geometry of the aquifers within the SLMS as well as its hydraulic parameters (transmissivity and storage coefficient). Indeed, pumping test analysis has pointed out the occurrence of impervious boundaries and the occurrence of different porosities (Fig. 6) in the flow system associated to the depositional units (specially, those with low hydraulic conductivity levels) and to the tectonic features of this mountain massif.

Hydrochemical and isotopic data provide an explanation of the groundwater flow path and of the relative transit times with the SLMS. Different hydrochemical facies illustrate the hydrochemical sequence that takes place within the system (Table 3). In general, most of the natural springs (group 'A') and some few wells present low EC and bicarbonate-calcium facies, which are indicative of low transit times within the system. Other groups show larger proportions of Mg, Na, Cl and SO_4 that are attributed to the effect of groundwater flowpaths through distinct stratigraphic formations, as pointed out by Mg occurrence and distribution. Indeed, Mg and SO_4 enrichment indicate the influence of dolomite dissolution, whereas Na enrichment is caused by cationic exchange (Fig. 10) in clay-rich strata. Given the geological mapping and cross-sections of the area, hydrochemical facies of the well samples are fully justified by the predominant rock type around the borehole and along the regional flow-paths (Fig. 13).

591 In this sense, meteoric water recharge would be characterized as a group ‘A’ facies in
592 the initial reach of the downward groundwater flow path. Infiltration through
593 conglomerates mainly generates a bicarbonate-calcium facies, constituting a local
594 hydrological system. As groundwater flows within the system, it becomes enriched in
595 Mg, Cl and/or Na; as, for instance, sample of ‘B’ group, which represents a more
596 evolved water within the alluvial fan area. Moreover, red sandstones and mudstones
597 (SMr), which are laterally between conglomerates (Cp, Cc) and grey sandstones (Sg)
598 layers, act as a low permeability boundary, impeding groups ‘A’ and ‘B’ waters to
599 continue its flow towards the Sg sandstones and other down-gradient locations.

600 Infiltration through megajoints is facilitated by the fracture network which also allows
601 hydraulic connection across low permeability layers. Eventually, bicarbonate-calcium
602 groundwater (group ‘A’) flows from alluvial fan conglomerates (Cp and Cc types) to
603 delta front conglomerates and sandstones (Cg and Sg types, respectively), generating
604 a second, large scale system. This happens basically in the upper part of the maximum
605 progradation episodes (see before), resulting in an enrichment of Mg, SO_4, Na and Cl
606 (groups ‘C’ and ‘D’ samples), and a depletion in Ca due to cation exchange processes,
607 that finally defines group ‘E’ groundwater samples. Therefore, flow towards the Sg
608 formations is due to the fracture network and some lateral progression of the Cp to Cg
609 types that overcome the low hydraulic conductivity unit represented by SMr layers
610 (Fig. 13). Recharge of the grey sandstone (Sg formation) also occurs by surface water
611 infiltration.

612 From a hydrochemical perspective, surface water atain (partial) equilibrium with
613 atmospheric conditions, and this may result in a loss of bicarbonate when it infiltrates
614 an mixes with groundwater (group ‘D’). Resulting water undergoes further equilibration
615 with the Sg formation lithology through water-rock interaction. Indeed, stream recharge
616 is reinforced in some locations near Talamanca by small dams built to retain water and
617 enhance infiltration.

Isotopic data supports the stated hydrochemical evolution. Groups ‘A’ and ‘B’ samples, which include all natural springs and few wells, show a small isotopic variability that may just represent the altitude range of the recharges areas in the SLMS. Hydrochemical and isotopic similarity of all natural springs suggest a fast transit time within the system. The compartmentalized nature of the aquifer system defines mesh-type geohydrological units limited by sedimentary discontinuities, as fine sediment strata, and fractures. Given the thick conglomeratic units where they appear, the distinct sets of fractures are visibly responsible for controlling such a local flow fields that discharge in natural springs. Locally, fracture flow may also discharge to eroding streams contributing to surface runoff as baseflow. Isotopic data from deep wells, represented by hydrochemical groups ‘C’ and ‘D’, show a clear evaporation trend which has been interpreted to be the result of a long pathway through the unsaturated zone/fracture systems before attaining the water table within the mountain range. Such recharge gets homogenized during its downward flow path as suggested by the allocation of the isotopic data along a single evaporation line. To some extent, the evaporation features of group ‘C’ samples could also be attributed to some temporary subaerial conditions, yet it is plausible that most of the evaporation (up to 5%) takes place in the unsaturated zone because it implies a longer residence time than the atmospheric exposure.

The hydrochemical enrichment of major ions, as mentioned for these groups, does not occur in the unsaturated zone. Instead, it takes place within the main conglomeratic fractured aquifer that occupies the central part of the SLMS (Cp and Cc formations), and within the delta front lithologies (Cg and Sg formations) as the flowpath advances. In other words, the final hydrochemical content of samples from deep wells is acquired in the central part of the SLMS, homogenized across the unsaturated zone, and completed within the aquifer, below the water table, in equilibrium with the dominant lithology. Dissolution of Mg-reach minerals, pyrite oxidation, clay weathering, and

645 cation exchange have been identified as the processes that contribute to their final
646 hydrochemical features. Transitory surface flow and its later reinfiltration to the aquifer
647 modifies the hydrochemical composition of same groundwater samples (group 'D'),
648 specially the carbonate system; although the final composition is clearly related to the
649 hosting rock.

650 In the distal part of the alluvial fan, the occurrence of mudstone layers imbedded in the
651 red sandstones (SMr) originates low hydraulic conductivity bodies, especially the grey-
652 blue mudstone unit (Mgb). In addition to the low permeability of these fine sediment
653 layers, fractures (interjoints) in sandstone are not hydraulically effective since they do
654 not propagate through the more plastic mudstone levels. Locally, the basinward
655 displacement of the sedimentary facies belt in the moment of maximum progradation
656 occasionally permited the sedimentation of conglomerates (Cg) in the marine zones
657 which hydraulically connect the alluvial conglomerates (Cp, Cc) with the marine
658 conglomerates and sandstones (Cg, Sg), providing an effective pathway for
659 groundwater flow. An example of such connection is found in S.LL-27 well, whose
660 discharge is significantly depended on one of the conglomerate Cg layers deposited
661 during a maximum progradation episode (Fig. 4).

662 More importantly, the distal evolution of Sg sandstones to Mgb mudstones, as well as
663 the interfingering of both rock-types, creates an important permeability barrier. This low
664 permeability boundary, assumed as impervious in a simple conceptual hydrogeological
665 model, impedes a groundwater flow further towards de NW, accordding to the main
666 flow direction controlled by the layer tilting. Such impervious depositional boundary acts
667 as a no-flow boundary and it determines the hydraulic head inside the entire SLMS
668 and, consequently, the groundwater storage of the system (Fig. 13).

669

670 **5-CONCLUSIONS**

671 The hydrogeological study of the Sant Llorenç de Munt alluvial fan system points out
672 the relevance of detailed, comprehensive geological knowledge to the understanding of
673 groundwater dynamics in this mountain area. In this study, stratigraphical,
674 sedimentological and tectonic data have provided the necessary information to build up
675 a geological scheme that explains recharge processes and flow paths. The key
676 geological features to understand groundwater paths within the system are vertical and
677 lateral sedimentary variability (sedimentary architecture) and specifically the
678 occurrence of low hydraulic conductivity units and no-flow limits, shown by the fracture
679 pattern analysis. In this study case, head levels provide limited, fragmentary
680 information because of the lack of monitoring boreholes in the inner part of the massif
681 and the occurrence of perched aquifers favoured by stratigraphic and tectonic features.
682 Pumping tests have also contributed to the understanding of the system. In addition of
683 the hydraulic parameters, drawdown data provide information about the response of
684 the system under exploitation and recharge. Identifying the occurrence of no-flow
685 boundaries, as in S.LL-27 deep well test, and double porosity within the aquifer layers
686 contributes to identify the main the aquifer geological features that govern groundwater
687 flow, and to figure out the extent of its potential exploitation.

688 Natural springs are highly valuable to understand the dynamics of the system and to
689 sample for hydrochemical and isotopic data. On one hand, isotopic data reveals a
690 compartmentalized system that recharges and drains groundwater on separate flow
691 subsystems that originate such springs. On the other hand, they also point out that a
692 significant recharge occurs through a thick unsaturated zone within the massif
693 accordding to the evaporation isotopic evidence found in the deepest wells in contrast
694 to that of natural springs. Furthermore, different hydrochemical facies can be clearly
695 defined accordding to the water chemical equilibrium with the distinct lithology of each
696 sedimentary unit.

Geological information validates the definition, first, of local scale flow systems which result in natural springs; that is, those that flow through compartments or blocks limited by sedimentary facies changes and fractures. Secondly, it also defines a large regional flow system that controls the overall regional groundwater flow to lateral formations and is constrained finally by low permeability units.

Geological formations as the Sant Llorenç de Munt mountain area, where the stratigraphical and tectonic structure outcrops and allows the understanding of its geological features, provide a valuable scheme to be used as reference for a groundwater resources efficient exploitation in similar buried systems. Despite the fracture pattern is important for aquifer connectivity, it should not be expected in unconsolidated fans (i.e, in recent, not lithified formations). In any case, sedimentary sequences mostly control the flow field. In this context, hydrochemical and isotopic data stands thus as a complementary and predictive tool to unveil flow characteristics even where limited logging and geological information is available.

ACKNOWLEDGMENTS

We thank the collaboration of water management companies in the area for their collaboration: Aigües de Manresa, Aigües de Terrassa and Sorea. We acknowledge the support provided and received by the municipalities of Mura, Talamanca, Pont Vilomara and Rocafort. We would like to thank the contribution of the “Catalana de Perforacions” and “Electrica Pintó” who have provided borehole logs, pumping test data, as well as inputs from owners and managers of several springs for private use. We also thank the valuable comments of the reviewers and Dr. Elizabeth Screaton for the editorial works.

This research was partially funded by Spanish Government project CGL2013-48869-C2-2-R and CGL2011-29975-c04-04, which continues under project CGL2014-57215-C4-2-R.

REFERENCES

Alsaker E, Gabrielsen RH, Roca E (1996) The significance of the fracture pattern of the Late-Eocene Montserrat fan-delta, Catalan Coastal Ranges (NE Spain). Tectonophysics 266: 465-491.

Anadón P (1978) El Paleogeno continental anterior a la transgresión Biarritziense (Eoceno medio) entre los ríos Gaià y Ripoll (Provincias de Tarragona y Barcelona). PhD Thesis, Facultat de Geologia, Universitat de Barcelona.

Anadón P, Cabrera L, Guimerà J, Santanach P (1985a) Paleogene strike-slip deformation and sedimentation along the southeastern margin of the Ebro Basin. In: Biddle KT and Christie-Blick N (eds) Strike-slip deformation, basin formation and sedimentation, 37. Society of Economic Paleontologists and Mineralogists, Special Publication. p 303-318.

Anadón P, Marzo M, Puigdefàbregas C (1985b) The Eocene fan delta of Montserrat (Southeastern Ebro Basin, Spain). Excursion 3, Field trip guidebook 6th European Regional Meeting I.A.S., Lleida, Spain..

Anders R, Mendez GO, Futa K, Danskin WR (2014) A geochemical approach to determine sources and movement of saline groundwater in a coastal aquifer. Ground Water, 52(5):756-68.

746 Andrés O (1964) Karstificación en conglomerados. Su estudio en el macizo de Sant
747 Llorenç del Munt - serra de l'Obac (Barcelona). Geo y Bio Karst 2: 9-12.

748 Anglés M (2013) Hidroestratigrafia del ventall deltaic de Sant Llorenç del Munt (Eocè
749 mig-superior, Conca de l'Ebre). PhD Dissertation, Universitat Autònoma de
750 Barcelona.

751 Anglés M, Maestro E (2010-2011) Els conglomerats de Sant Llorenç del Munt (Eocè
752 mitjà-superior). Butlletí de la Institució Catalana d'Història Natural 76: 71-82.

753 Arenas C, Millán H, Pardo G, Pocoví A (2001) Ebro Basin continental sedimentation
754 associated with late compressional Pyrenean tectonics (north-eastern Iberia):
755 controls on basin margin fans and fluvial systems. Basin Research 13: 65-89.

756 Benvenuti M (2003) Facies analysis and tectonic significance of lacustrine fan-deltaic
757 successions in the Pliocene-Pleistocene Mugello Basin, Central Italy.
758 Sedimentary Geology 157: 197-234.

759 Blair TC (2000) Sedimentology and progressive tectonic unconformities of the
760 sheetflood-dominated Hell's Gate alluvial fan, Death Valley, California.
761 Sedimentary Geology 132: 233-262.

762 Brusi D, Ramonell C, Menció A, Roqué C, Mas-Pla J (2011) Isotopic characterization of
763 ground water in western Pyrenees. 9th Int. Symposium on Applied Geochemistry.
764 Tarragona. Abstracts book.

765 Cabello P, Falivene O, López-Blanco M, Howell J, Arbués P, Ramos E (2011) An
766 outcrop-based comparison of facies modelling strategies in fan-delta reservoir
767 analogues from the Eocene Sant Llorenç del Munt fan-delta (NE Spain).
768 Petroleum Geoscience 17: 65-90.

769 Carmona JM, Bitzerb K, López E, Bouazza M (2000) Isotopic composition and origin of
770 geothermal waters at Caldetes (Maresme—Barcelona). Journal of Geochemical
771 Exploration 69–70: 441–447

772 Carrillo-Rivera JJ, Irén Varsányi I, Kovács LO, Cardona A (2007) Tracing groundwater
773 flow systems with hydrogeochemistry in contrasting geological environments.
774 Water Air and Soil Pollution 184: 77–103.

775 Chapius, RP (1994). Assessment of Methods and Conditions to Locate Boundaries: I.
776 One or Two Straight Impervious Boundaries. Groundwater, 32(4): 576–582.

777 Chen W-F, Liu T-K (2003) Dissolved oxygen and nitrate of groundwater in Choshui
778 Fan-Delta, western Taiwan. Environmental Geology 44:731–737

779 Chen W-F, Liu T-K (2005) Ion activity products of iron sulphides in groundwaters:
780 implications from the Choshui fan-delta, Western Taiwan. Geochimica et
781 Cosmochimica Acta 69 (14): 3535–3544

782 Craig H (1961) Isotopic variations in meteoric waters. Science 133: 1702-1703.

783 DeCelles PG, Gray MB, Ridgway KD, Cole RB, Pivnik DA, Pequera N, Srivastava P
784 (1991) Controls on synorogenic alluvial-fan architecture, Beartooth Conglomerate
785 (Palaeocene), Wyoming and Montana. Sedimentology 38: 567-590.

786 Epstein S, Mayeda T (1953) Variation of O 18 content of waters from natural sources.
787 Geochimica et cosmochimica acta 4(5): 213-224.

788 Folch A, Menció A, Puig R, Soler A, Mas-Pla J (2011) Groundwater development
789 effects on different scale hydrogeological systems using head, hydrochemical
790 and isotopic data and implications for water resources management: The Selva
791 basin (NE Spain). Journal of Hydrology 403 (1-2): 83-102

792 Freixes A (1986) El carst conglomeràtic experimental de Rellinars: un enfocament
793 sistèmic i hidrogeològic en la recerca del medi càrstic. Research Project, Facultat
794 de Geologia, Universitat de Barcelona.

795 Galloway WE, Hobday DK (1996). Terrigenous Clastic Depositional Systems:
796 Applications to Fossil Fuel and Groundwater Resources, Springer, 2nd ed.

797 Gonfiantini R (1986) Environmental isotopes in lake studies. In: Fritz P, Fontes JCh
798 (eds) Hanbook of Environmental Isotope Geochemistry.Elsevier 2: 113-168.

799 Grau A, Castells R, Deu M, Guàrdia A, Guerrero C, Roijals X, Burriel JA, Ibàñez JJ,
800 Pons X (2007) El mapa de cobertes del sòl de Catalunya com a eina d'estudi de
801 Sant Llorenç del Munt i l'Obac. VI Trobada d'Estudiosos de Sant Llorenç del
802 Munt i l'Obac. Diputació de Barcelona.

803 Harvey AM, Mather AE, Stokes M (2005) Alluvial fans: geomorphology, sedimentology,
804 dinamics - introduction. A review of alluvial-fan research. In: Alluvial fans:
805 geomorphology, sedimentology, dinamics (Harvey AM, Mather AE, Stokes M
806 (eds). Geological Society of London, special publication 251: 1-7.

807 ICGC (2003) Mapa Geològic de Catalunya 1:25 000, Full 392-1-1 (71-29) Monistrol de
808 Montserrat. Institut Cartogràfic i Geològic de Catalunya, Barcelona.

809 ICGC (2010) Mapa geològic de Catalunya, Geotreball I, Mapa geològic 1:25.000 - Full
810 363-2-2 (72-28) Sant Llorenç Savall. Institut Cartogràfic i Geològic de Catalunya,
811 Barcelona.

812 ICGC (2011a) Mapa geològic de Catalunya, Geotreball I, Mapa geològic 1:25.000 - Full
813 392-2-1 (72-29) Castellar del Vallès. Institut Cartogràfic i Geològic de Catalunya,
814 Barcelona.

815 ICGC (2011b) Mapa geològic de Catalunya, Geotreball I, Mapa geològic 1:25.000 - Full
816 363-1-2 (71-28) Manresa. Institut Cartogràfic i Geològic de Catalunya, Barcelona.

817 IDESCAT (2016) El municipi en xifres, Institut d'Estadística de Catalunya,
818 http://www.idescat.cat/emex, Cited 16 february 2017.

819 Lambán J, Custodio E (1999) Estudio isotópico ambiental (o18-d) en la Unidad Anoia:
820 Principales zonas de recarga e implicaciones en el funcionamiento
821 hidrogeológico del Sistema. Ingeniería del Agua 6(2): 139-150.

822 Li J, Li F, Liu Q, Zhang Y (2014) Trace metal in surface water and groundwater and its
823 transfer in a Yellow River alluvial fan: Evidence from isotopes and
824 hydrochemistry. Science of the Total Environment 472: 979-988, doi
825 10.1016/j.scitotenv.2013.11.120

826 Lindholm RC, Finkelman RB (1972) Calcite staining: semiquantitative determination of
827 ferrous iron. Journal of Sedimentary Research 42 (1): 239-242.

828 Llopis N (1944) Morfoestructura de los relieves de pundingas de Sant Llorenç del Munt
829 - serra de l'Obac (Barcelona). Estudios Geográficos 17: 687-814.

830 López-Blanco M (1994) Estructuras contractivas de la Cordillera Prelitoral Catalana
831 entre la sierra de Les Pedritxes y el río Ripoll: evolución y relación con los
832 depósitos del márgen de la cuenca del Ebro. Geogaceta 16: 43-46.

833 López-Blanco M (1996) Estratigrafía secuencial de sistemas deltaicos en cuencas de
834 antepaís: ejemplos de Sant Llorenç del Munt, Montserrat y Roda (Paleógeno,
835 cuenca de antepaís surpireanica). PhD Dissertation, Universitat de Barcelona,
836 238 pp.

837 López-Blanco M (2006) Stratigraphic and tectonosedimentary development of the
838 Eocene Sant Llorenç del Munt and Montserrat fan-delta complexes (Southeast
839 Ebro basin margin, Northeast Spain). Contributions to Science 3 (2): 125-148.

840 Maestro E (1987) Estratigrafia i fàcies del complex deltaic (Fan delta) de Sant Llorenç
841 del Munt (Eocè mig-superior. Catalunya). PhD Thesis, Facultat de Ciències,
842 Universitat Autònoma de Barcelona, Bellaterra.

843 Mas-Pla J, Bach J, Viñals E, Trilla J, Estalrich J (1999) Salinization processes in a
844 coastal leaky aquifer (Alt Empordà, NE Spain). Physics and Chemistry of the
845 Earth, Part B: Hydrology, Oceans & Atmosphere, 24(4): 337-341.

Mas-Pla J, Menció A, Bach J, Soler D, Zamorano M, Brusi D (2016) Trace element groundwater pollution hazard in regional hydrogeological systems (Empordà basin, NE Spain). Water, Soil & Air Pollution, 227:218-240.

Mata-Perelló JM (1990) Els minerals de Catalunya. Institut d'Estudis Catalans, Barcelona, 441 pp.

Menció A, Mas-Pla J, Otero N, Regàs O, Boy-Roura M, Puig R, Bach J, Domènech C, Zamorano M, Brusi D, Folch A (2016) Nitrate pollution of groundwater; all right …, but nothing else? Science of the Total Environment, 539C: 241-251.

Neal C, Neal M, Warrington A, Avila A, Pinol J, Roda F (1992) Stable hydrogen and oxygen isotope studies of rainfall and streamwaters for two contrasting holm oak areas of Catalonia, northeastern SpainJournal of Hydrology 140: 163–178.

Otero N, Canals A, Soler A (2007) Using dual-isotope data to trace the origin and processes of dissolved sulphate: a case study in Calders stream (Llobregat basin, Spain). Aquatic Geochem 13: 109-126.

Peng T-R, Lu W-C, Chen K-Y, Zhan W-J, Liu T-K (2014) Groundwater-recharge connectivity between hills-and-plains área of western Taiwan using wáter isotopes and electrical condctivity. Journal of Hydrology 517: 226-235.

Plata Bedmar A (1994) Composición isotópica de las aguas subterráneas de la Península Ibérica. Centro de Estudios y Experimentación de Obras Públicas. Madrid, Pub. M-39.

Renard P, Glenz D, Mejias M (2009) Understanding diagnostic plots for well-test interpretation. Hydrogeology Journal, 17 (3): 589-600.

RURALCAT (2017) Dades meteorològiques, La comunitat virtual agroalimentària i del món rural, Generalitat de Catalunya, http://www.ruralcat.net/web/guest/reg.dadesmeteo, Cited 16 february 2017.

871 Sohn YK, Rhee CW, Kim BC (1999) Debris flow and hyperconcentrated flood-flow
872 deposits in a alluvial fan, Northwestern part of the Cretaceous Yongdong Basin,
873 Central Korea. The Journal of Geology 107: 111-132.

874 Tóth J (1995) Hydraulic continuity in large sedimentary basins. Hydrogeology Journal
875 3: 4-16.

876 Tóth J (2000) Las aguas subterráneas como agente geológico: Causas, procesos y
877 manifestaciones. Boletín Geológico y Minero 111 (4): 9-26.

878 Tsang CF, McEdwards DG, Narashiman TN, Witherspoon PA (1977) Variable Flow
879 Well-Test Analysis by a Computer-Assisted Matching Procedure. Paper No.
880 6547, 47th Annual Western Regional Meeting, SPE of AIME, Bakersfield,
881 California.

882 Yechieli Y, Shalev E, Wollman S, Kiro Y, Kafri U (2010). Response of the
883 Mediterranean and Dead Sea coastal aquifers to sea level variations.Water
884 Resources Research 46: 1-11

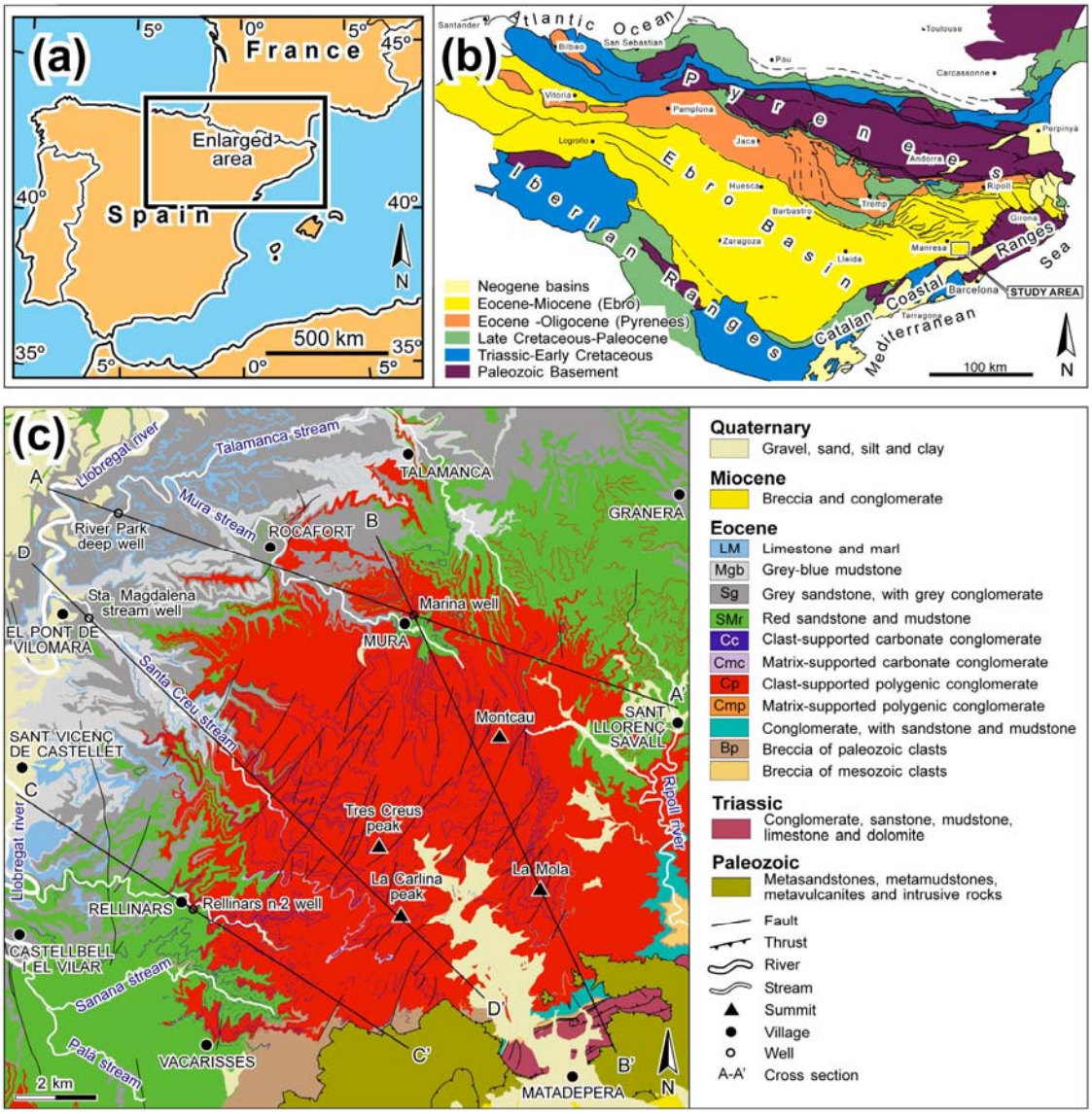

Fig. 1 a, **b** Geographical and geological setting of the Ebro Basin; **c** Geological map of the study area.

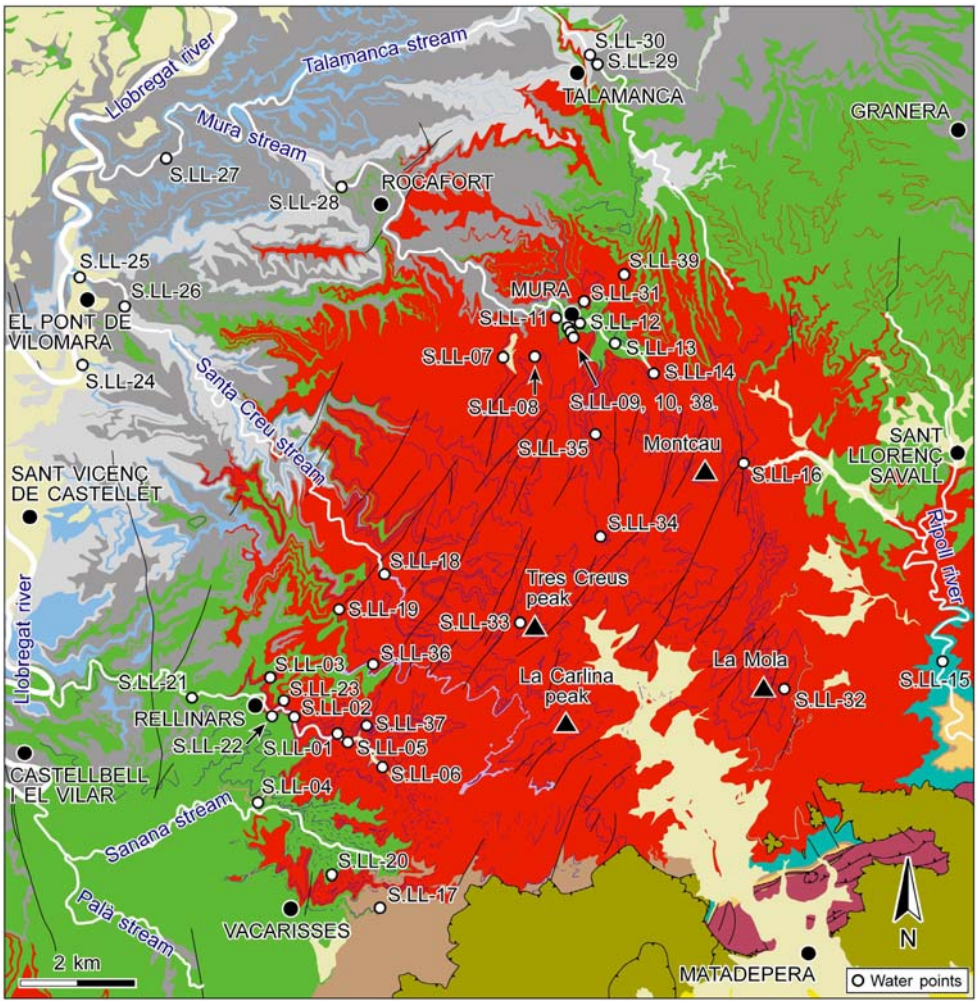

Fig. 2 Location of the water points studied at the Sant Llorenç del Munt fan delta (legend as in Fig. 1c).

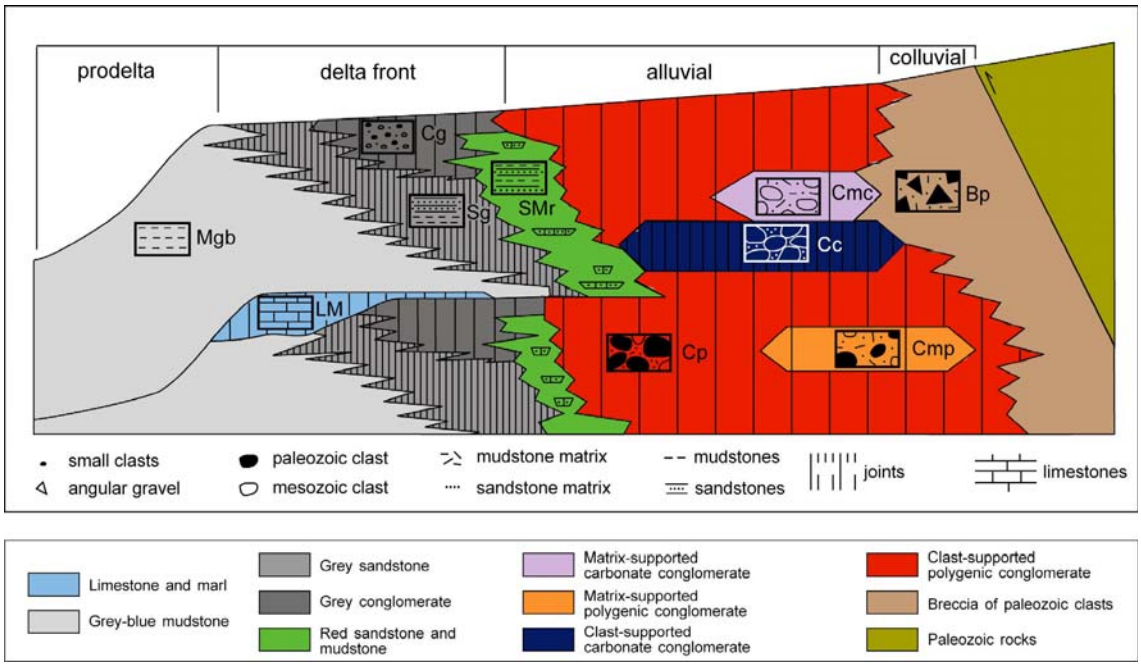

Fig. 3 Depositional environments of the Sant Llorenç del Munt fan delta with the main lithological features of the rock types. Fracture density is represented by differently spaced vertical lines.

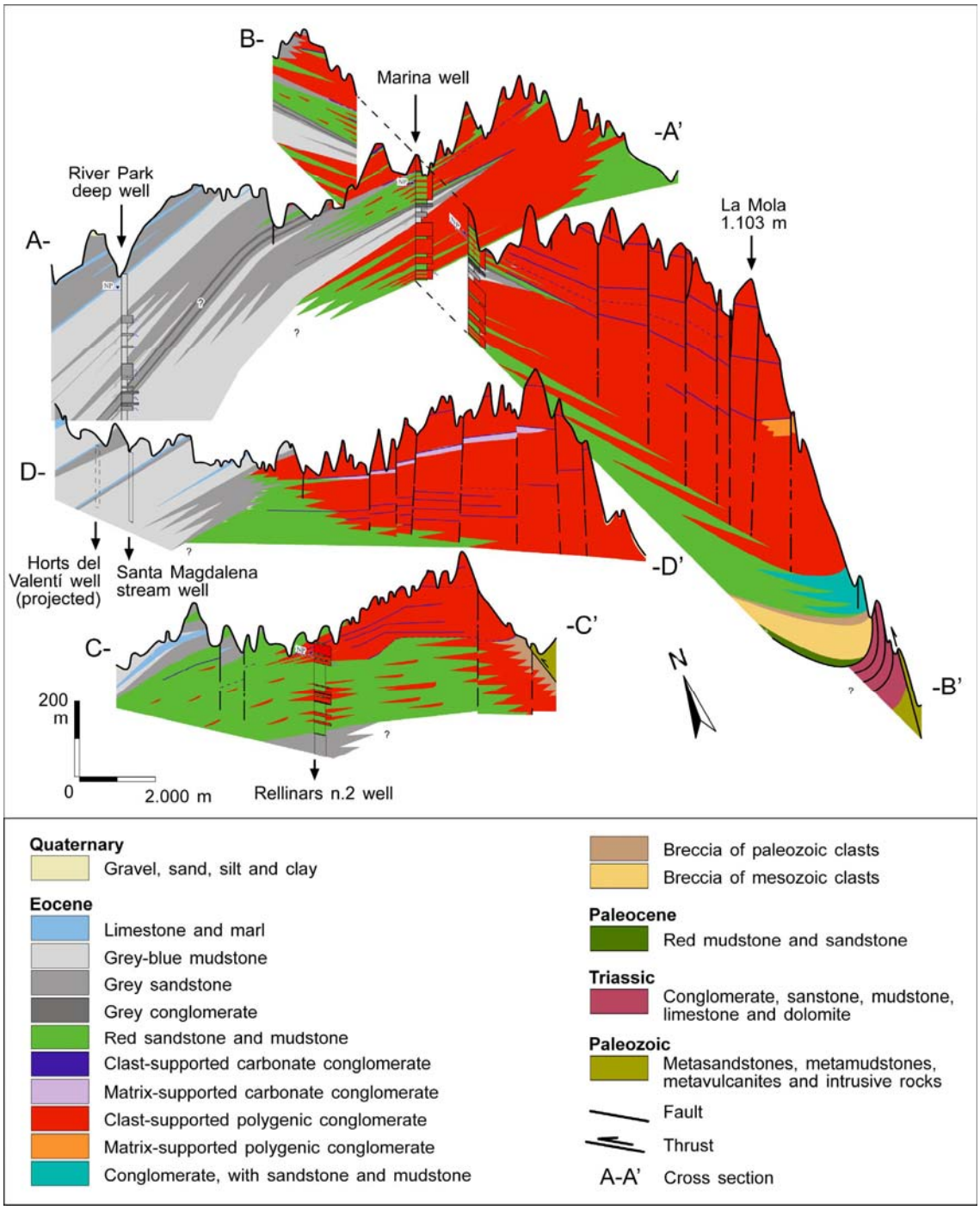

Fig. 4 Cross sections along the Sant Llorenç del Munt fan delta (see location in Fig. 1c).

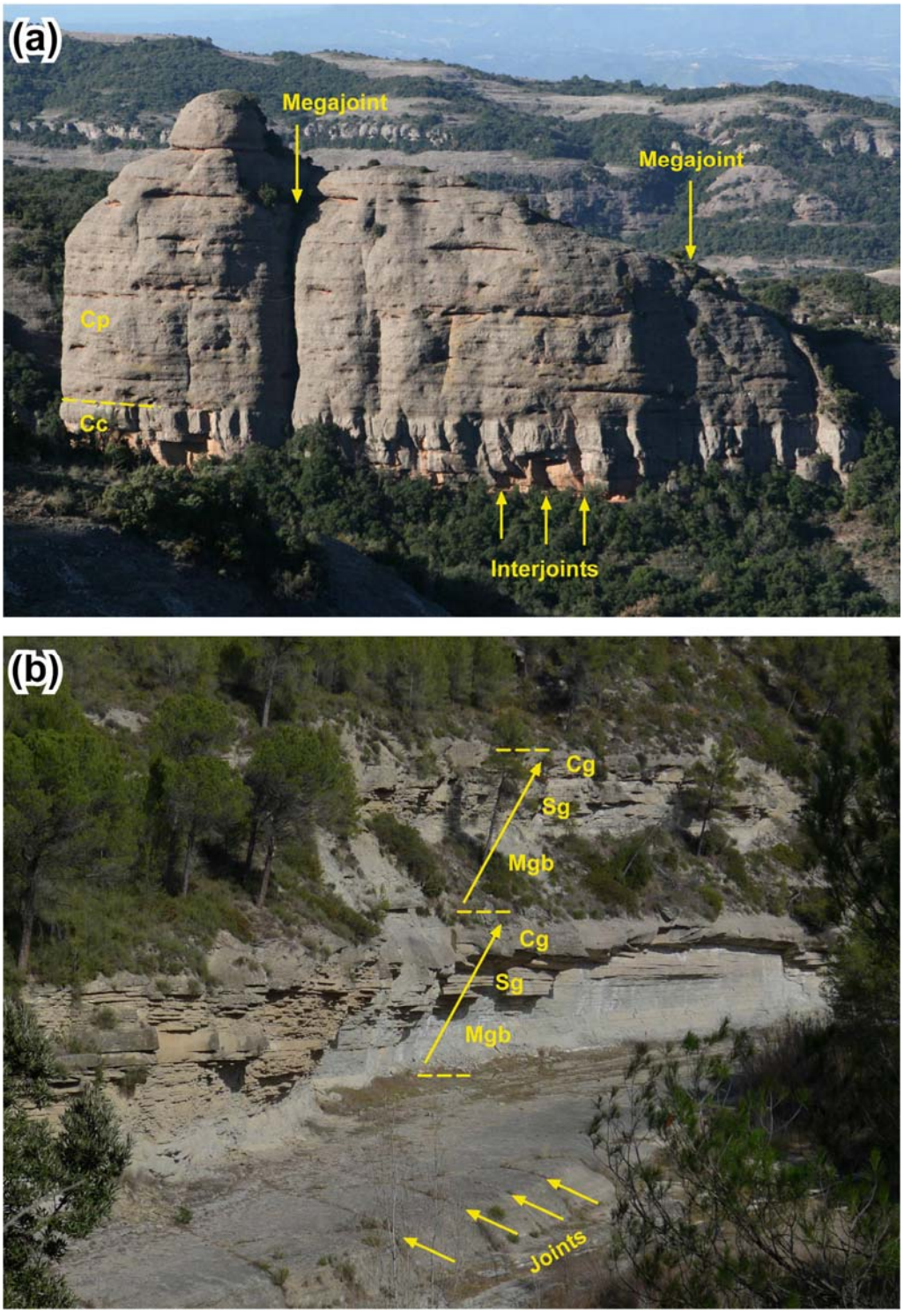

Fig. 5 a The Falconera cliff display megajoints affecting both Cp and Cc, and interjoints affecting solely the Cc bed; **b** The Talamanca stream display the thickening and coarsening upwards front deltaic sequences which show the following order (from base to top): Mgb, Sg and Cg.

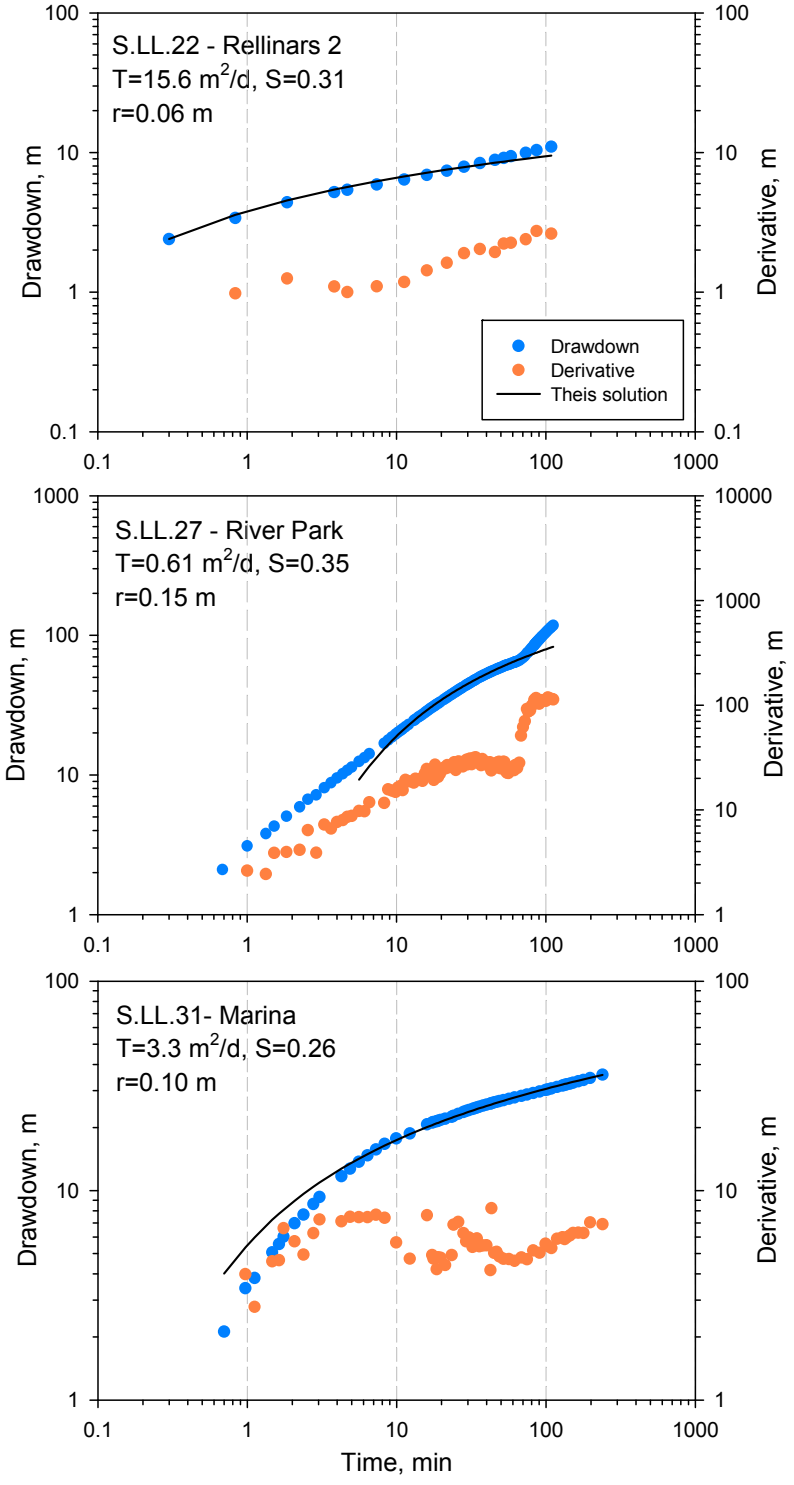

Fig. 6 Diagnostic analysis using log-log plots of the pumping tests conducted at constant discharge rate. Drawdown data are plotted jointly with thir derivatives, and fitted Theis solution.

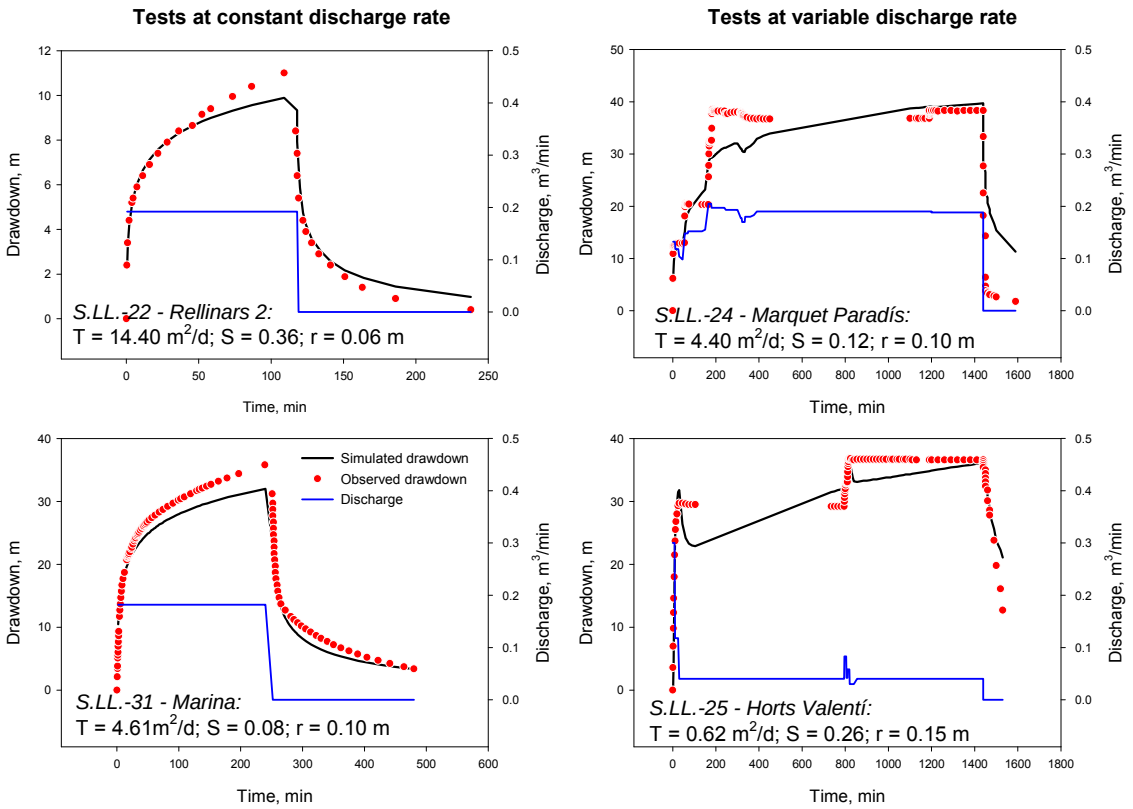

922

923

924 **Fig. 7** Pumping tests at wells S.LL-22, 24, 31, 25 using a variable discharge approach
925 (to include pumping rate variations as well as the recovery part) to fit T and S values
926 according to Theis solution (see text).

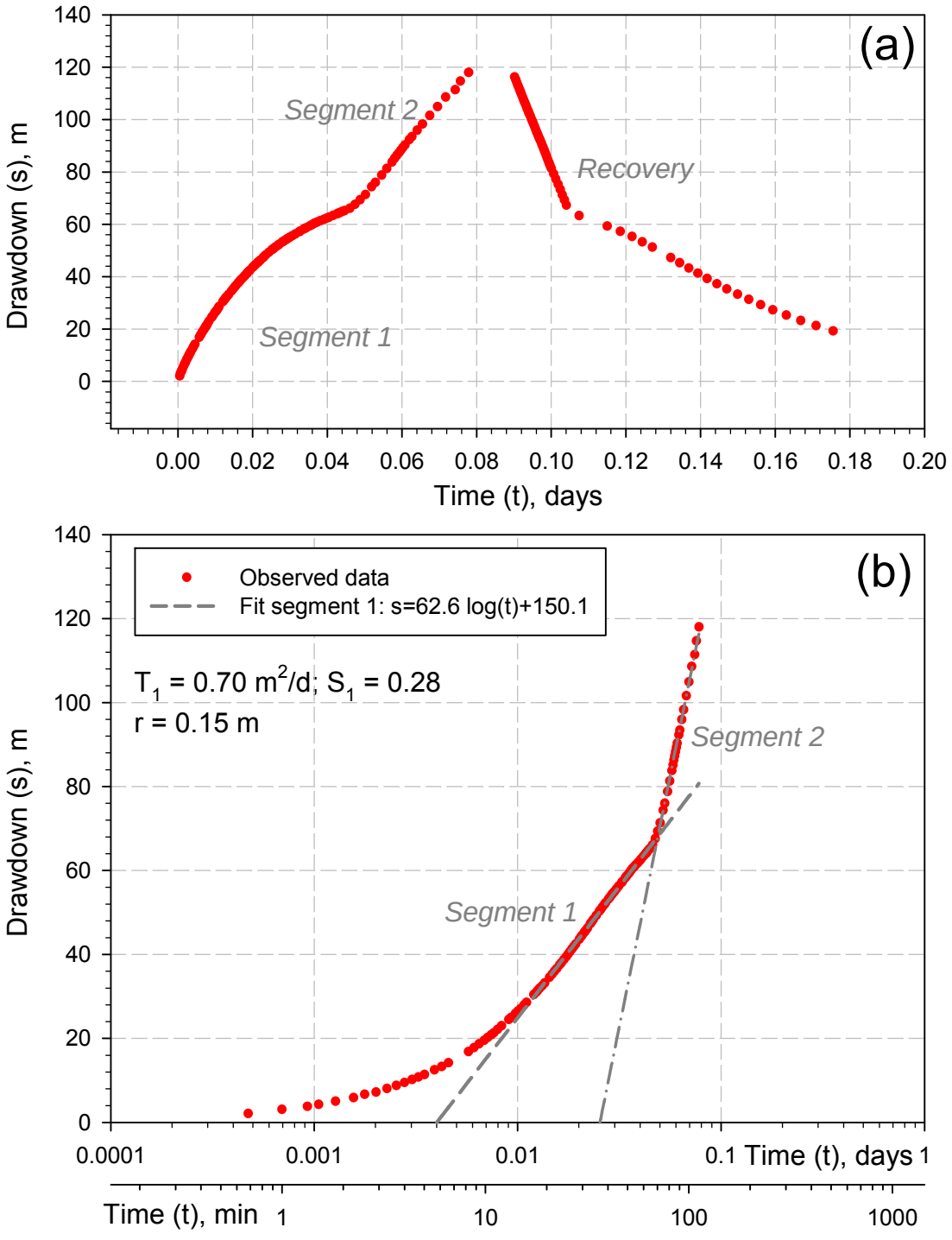

Fig. 8 a Drawdown and recovery data at the S.LL-27 (River Park), and **b** pumping test analysis using the Cooper-Jacob method.

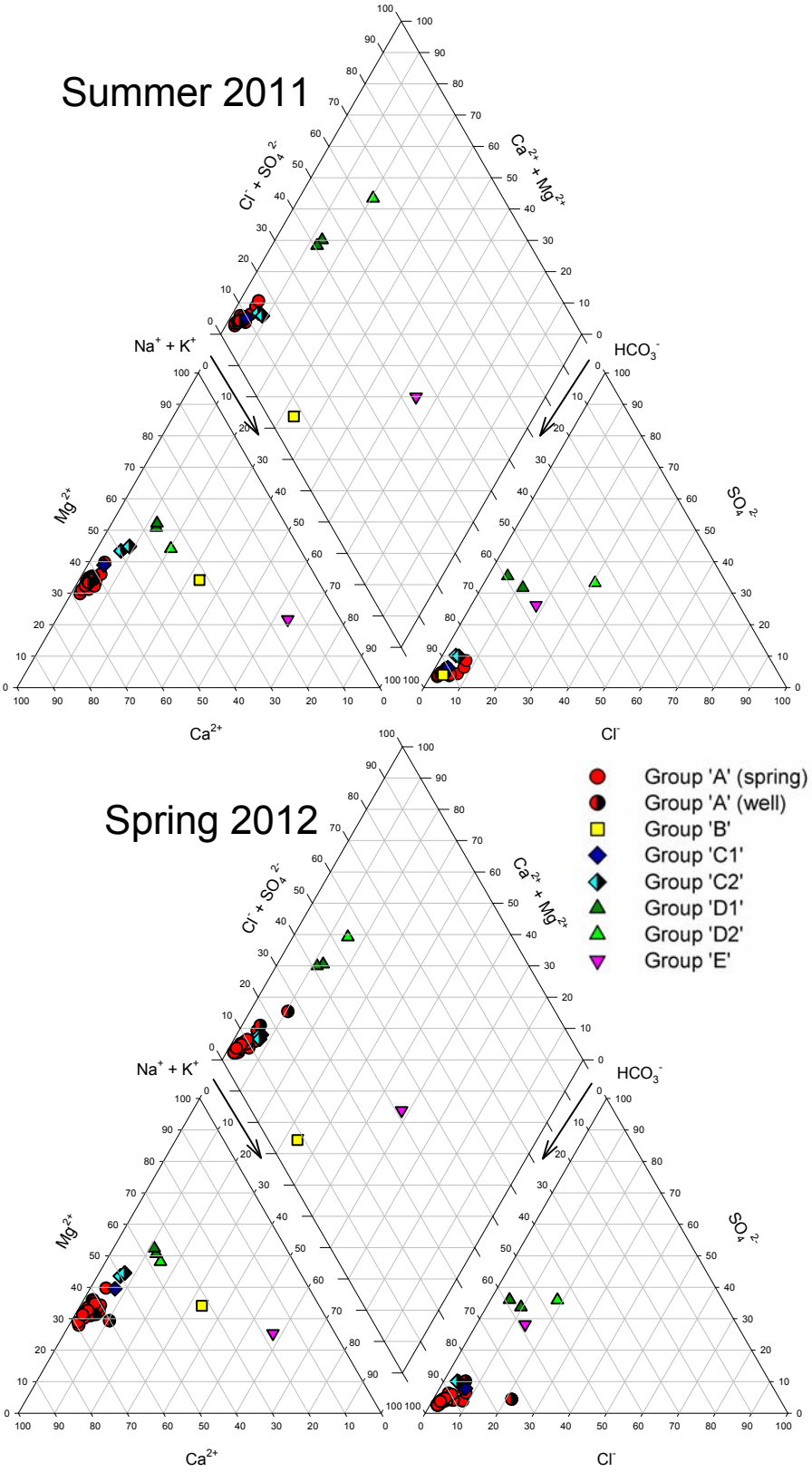

932

933 **Fig. 9** Piper diagrams from summer 2011 and spring 2012 surveys.

934

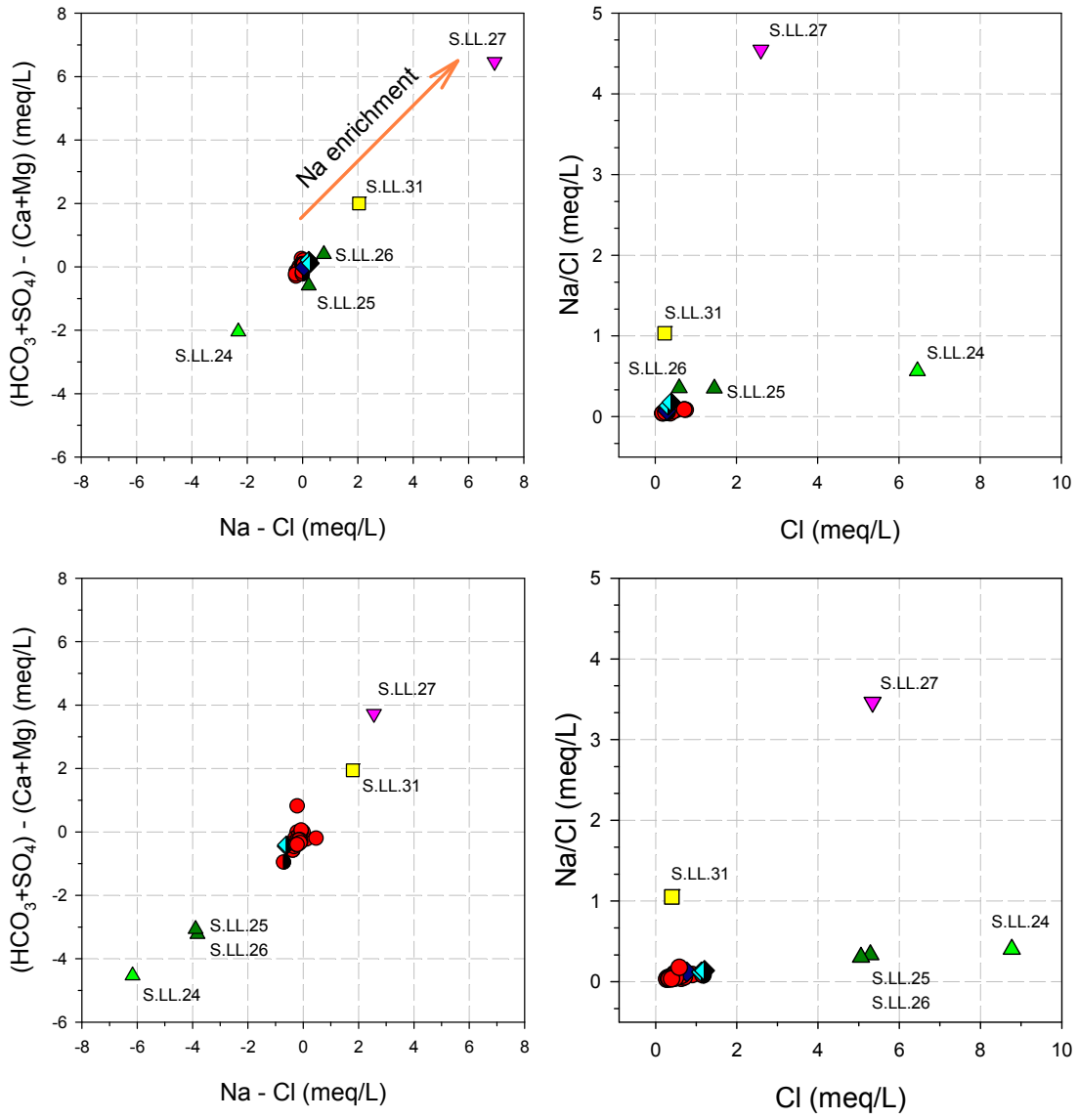

935

936

937 **Fig. 10** Binary plots related to the cation exchange Na-Ca, expressed as a difference of
938 the main major constituents, and of the ratio Na/Ca vs Cl for the 2011 and 2012
939 surverys (up and bottom, respectively).

940

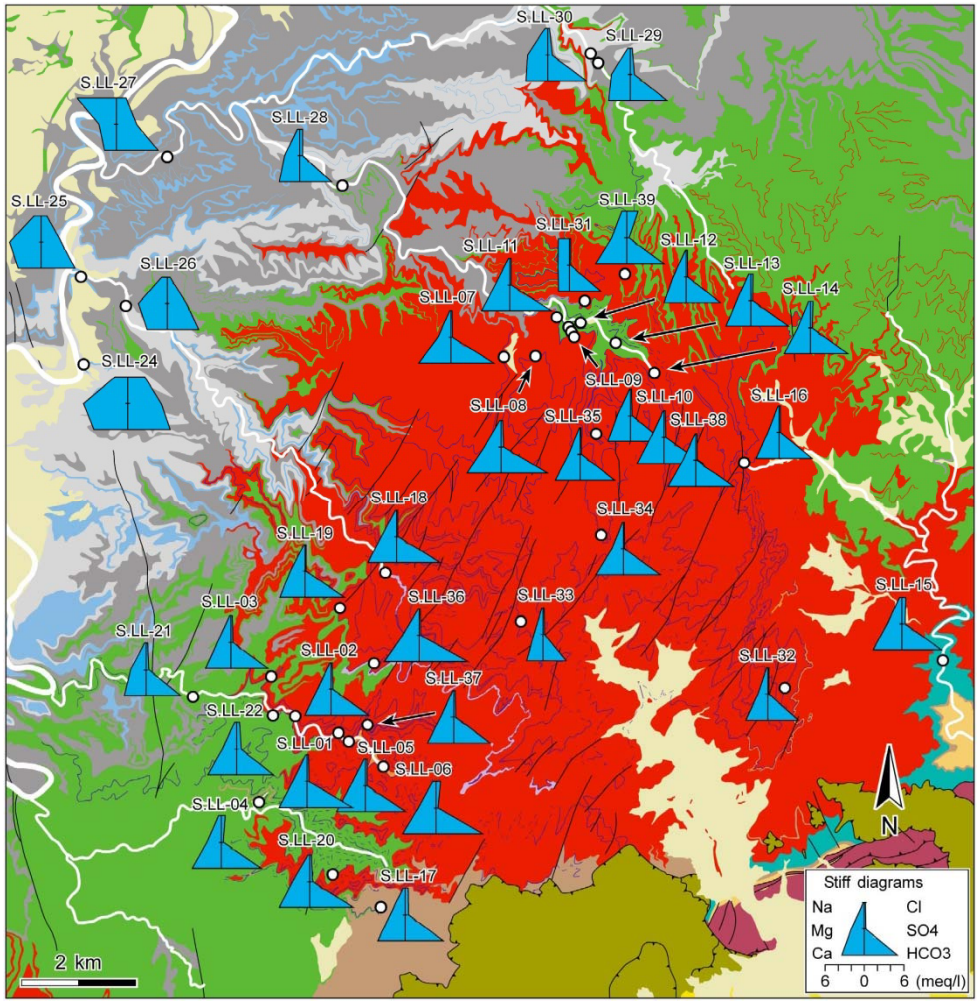

941

942

943 **Fig. 11** Stiff diagrams from spring 2012 field campaign (geological legend as in Fig.
944 1c).

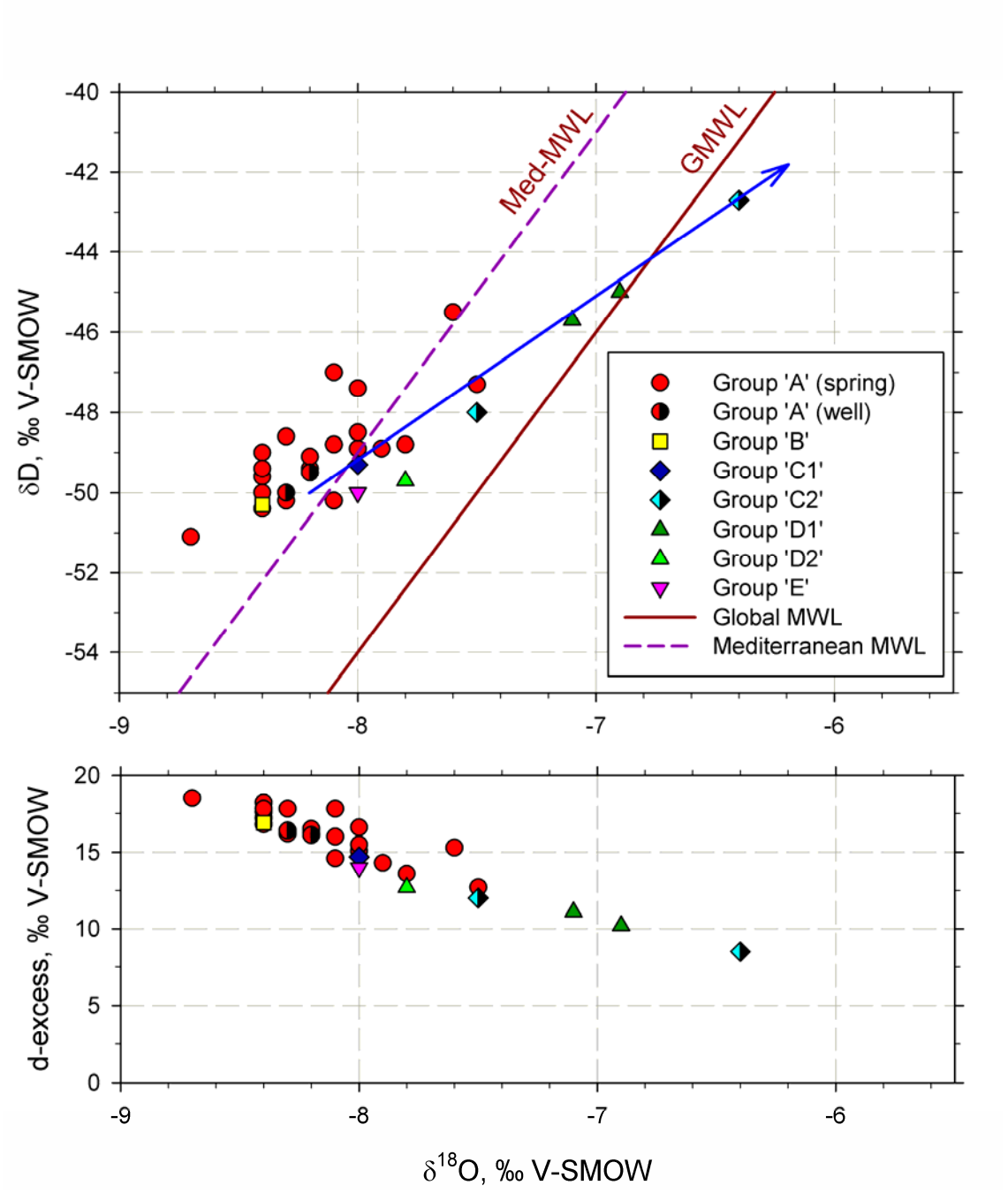

Fig. 12 Relationship $\delta D/\delta\ ^{18}O$ of the summer 2011 field campaign, with the representation of the Global and Mediterranean Meteoric Water Lines (MWL). The blue arrow represents a potential evaporation trend with an approximate origin at $\delta^{18}O$ = -8.2‰, δD = -50‰. Unless indicated (as for Group A), samples belong to wells.

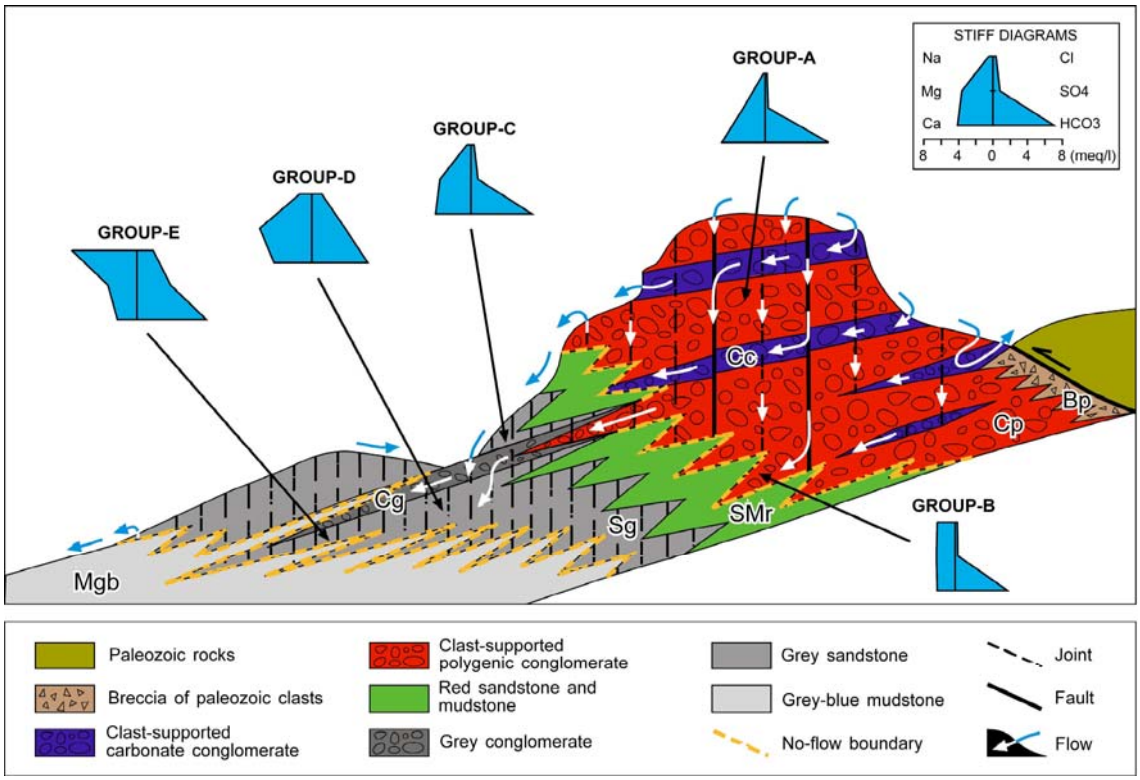

Fig. 13 Conceptual hydrogeological model for the SLMS and evolutionary relationships among the different hydrochemical groups. Mountains to the right represents the main recharge area. Geology has been simplified to show the hydrogeochemical evolution from the conglomerate units towards other lithological formations that modify groundwater composition due to water-rock interactions.

Table 1 Main lithofacies of the Sant Llorenç del Munt with summarized features.

ROCK TYPES	LITOLOGY & COLOR	TEXTURE / SELECTION	GRANULOMETRY	PERCENTAGE OF WHOLE ROCK MINERALOGY *	MORPHOLOGY OF SEDIMENTARY BODIES	INTERNAL STRUCTURES	GENETIC INTERPRETATION	DEPOSITIONAL ENVIRONMENT	FRACTURATION (m/ joints)
Breccia of paleozoic clasts (Bp)	Mudstone and sandstone breccia, dark red or brown	Matrix-supported to clast-supported	Clast: max 20-28 cm. Matrix: mud-sand	SIL: 98.8, CAL: 1.2	Lenticular. Thickness: dm-m. Continuity: hm	Disorganized or fining upward	Debris flow	Colluvial	Poorly defined
Clast-supported polygenic conglomerate (Cp)	Dark red conglomerate	Clast-supported	Clast: max 160 cm. Matrix: sand with little mud	SIL: 69.9, CAL: 5.8, DOL: 24.2, OTHERS: 0.1	Tabular or channelized. Thickness: max 2,2 m. Continuity: m-dam	Horizontal bedding and cross bedding	Aqueous flow: laminar, braided or with some sinuosity	Proximal and distal alluvial fan	8.1 35.0 37.3 87.5
Clast-supported carbonate conglomerate (Cc)	Grey conglomerate		Clast: max 100 cm. Matrix: sand	SIL: 19.2, CAL: 13.4 DOL: 67.3, OTHERS: 0.1	Tabular or channelized. Thickness: max 1,7 m. Continuity: m-dam	Horizontal bedding and cross bedding	Aqueous flow: laminar to braided		5.2 6.2 6.3 8.6
Matrix-supported polygenic conglomerate (Cmp)	Sandstone-mudstone conglomerate, red	Matrix-supported	Clast: max 200 cm. Matrix: sand-mud	SIL: 73.7, CAL: 3.4, DOL:22.2, OTHERS: 0.7	Tabular or lenticular. Thickness: max 2,6 m. Continuity: m-hm	Coarsening upward, fining upward or disorganized	Debris flow to hyperconcentrated flow	Proximal alluvial fan	Poorly defined
Matrix-supported carbonate conglomerate (Cmc)	Sandstone-mudstone conglomerate, red-orange		Clasts: max 380 cm. Matrix: sand-mud	SIL: 42.6, CAL: 8.2, DOL:47.9, OTHERS: 1.3	Tabular or lenticular. Thickness: max 3,8 m. Continuity: m-hm	Coarsening upward, fining upward or disorganized			
Red sandstone and mudstone (SMr)	Sandstone and mudstone, red	Very poorly sorted to moderately sorted	Sand-mud and mud	Sandstone: SIL: 90.9, CAL: 5.1, DOL: 1.0, OTHERS: 3.0	Tabular, lenticular or wavy sandstone, alternate with mudstone. Thickness: cm-m. Continuity: m-hm	Massive, fining upward, horizontal bedding and cross bedding	Aqueous flow: sheet flood and overflow channel	Distal alluvial fan	0.4 0.7 1.2
Grey conglomerate (Cg)	Grey conglomerate	Clast-supported or matrix-supported	Clast: cm order. Matrix: sand with little mud	SIL: 68.8, CAL: 8.8, DOL: 20.4, OTHERS: 1.9	Tabular to lenticular. Thickness: dm-m. Continuity: dam-hm	Cross bedding	Aqueous flow of distributary mouth bar	Delta front	2.2 2.5
Grey sandstone (Sg)	Grey sandstone	Moderately sorted to very well sorted	Sand	SIL: 55.6, CAL:29.3, DOL:5.1, OTHERS: 10.1	Tabular, lenticular or wavy. Thickness: cm-m. Continuity: dam-hm	Horizontal bedding and cross bedding	Aqueous flow of distributary mouth bar		0.9 2.7
Grey-blue mudstone (Mgb)	Carbonated mudstone or marl, grey-blue	---	Silt and/or clay	Highly variable (carbonate and clays)	Tabular	Massive	Decantation	Prodelta	Poorly defined
Limestone and marl (LM)	Grey limestone and blue-grey marl	Packstone, grainstone o boundstone		Limestone: SIL: 13.1, CAL: 84.8, DOL: 0.0, OTHERS: 2.0	Tabular	Massive, nodular bedding or organic structure	Biochemical carbonate precipitation	Carbonate platform	2.4 4.8

* Mineralogical composition as percentage of: silicate minerals (SIL), calcite (CAL), dolomite (DOL), and opaque minerals and organic matter (OTHERS). After Anglés (2013).

Table 2 Synthesis of the aquifers levels and hydraulic parameters of wells. Aquifer levels refer to the screened intervals in each well.

WELL	Depth (m)	LITHOSTRATIGRAPHIC UNITS (m deep)		AQUIFERS LEVELS (m depth)	PIEZOMETRIC LEVEL (m deep)	PUMPING DISCHARGE (m^3/d)	PUMPING TIME / RECUPERATION TIME (d)	TRANSMISSIVITY (m^2/d)	STORAGE COEFFICIENT
S.LL.-22 Rellinars n.2	300	0-30	Cp	45-54	29.60	240	0.08 / 0.08	14.40 - 15.60	0.31-0.36
		30-33	SMr						
		33-42	Cp						
		42-45	SMr						
		45-54	Cp						
		54-245	SMr + Cp						
		245-300	Sg						
S.LL.-31 Marina	335	0-51	Cp + SMr	309-320	98.28	240	0.17 / 0.16	3.30 – 4.61	0.08 – 0.26
		51-54	Sg						
		54-130	Cp + SMr						
		130-181	Cg + Sg + Mgb						
		181-335	Cp + SMr						
S.LL.-24 Marquet Paradís	51	0-8	Quaternary deposits	12-13 33-36 42-48	9.58	variable	1 / 0.10	4.40	0.12
		8-33	Mgb						
		33-45	Sg						
		45-51	Mgb						
S.LL.-25 Horts Valentí	164	Sg and Mgb		---	11.13	variable	1 / 0.06	0.62	0.26
S.LL.-27 River Park	389	0-109	Mgb	109-130 157-163 190-196 239-272 275-281 312-348 354-363	43.70	240	0.09 / 0.17	0.61-0.70	0.28-0.35
		109-130	Sg						
		130-157	Mgb						
		157-163	Sg						
		163-190	Mgb						
		190-196	Sg						
		196-239	Mgb						
		239-272	Sg						
		272-275	Mgb						
		275-281	Sg						
		281-312	Mgb + Sg						
		312-348	Sg + Cg						
		348-351	Mgb						
		351-363	Sg						
		363-389	Mgb						

Table 3.- Main features of hydrochemical groups.

HYDROCHEMICAL GROUPS		SAMPLING POINTS	NUMBER OF SAMPLES	HYDROCHEMICAL FACIES	MAIN PRODUCTIVE LITHOFACIES	DEPOSITIONAL ENVIRONMENT
A		All springs, wells Rellinars n.2 and n.3, Comes.	31	HCO_3-Ca	Cp + SMr	Alluvial fan
B		Marina well	1	HCO_3-Ca-Mg-Na		
C	C1	Rocafort well	1	HCO_3-Ca (↑Mg)	Quaternary deposits	Delta front
	C2	Wells Recàrrega, Dipòsit	2	HCO_3-Ca-Mg	Sg	
D	D1	Wells Sta. Magdalena stream, Horts Valentí	2	HCO_3-Mg		
	D2	Marquet Paradís well	1	HCO_3-SO_4-Mg-Ca		
E		River Park deep well	1	HCO_3-Na		